LAMINAR FLOW FORCED CONVECTION HEAT TRANSFER BEHAVIOR OF PHASE CHANGE MATERIAL FLUID IN STRAIGHT AND STAGGERED PIN MICROCHANNELS

A Thesis

by

SATYANARAYANA KONDLE

Submitted to the Office of Graduate Studies of
Texas A&M University
in partial fulfillment of the requirements for the degree of

MASTER OF SCIENCE

August 2010

Major Subject: Mechanical Engineering

LAMINAR FLOW FORCED CONVECTION HEAT TRANSFER BEHAVIOR OF PHASE CHANGE MATERIAL FLUID IN STRAIGHT AND STAGGERED PIN MICROCHANNELS

A Thesis

by

SATYANARAYANA KONDLE

Submitted to the Office of Graduate Studies of
Texas A&M University
in partial fulfillment of the requirements for the degree of

MASTER OF SCIENCE

Approved by:

Chair of Committee,	Jorge Alvarado
Committee Members,	Sai C. Lau
	Hamn-Ching Chen
Head of Department,	Dennis O'Neal

August 2010

Major Subject: Mechanical Engineering

ABSTRACT

Laminar Flow Forced Convection Heat Transfer Behavior of Phase Change Material Fluid in Straight and Staggered Pin Microchannels. (August 2010)

Satyanarayana Kondle, B.Tech., Indian Institute of Technology Madras

Chair of Advisory Committee: Dr. Jorge Alvarado

Microchannels have been studied extensively for electronic cooling applications ever since they were found to be effective in removing high heat flux from small areas. The rate of heat removed using microchannels depends on many factors including the geometry shape, solid and fluid materials used, and surface roughness, among others. Many configurations of microchannels have been studied with various materials and compared for their effectiveness in heat removal. However, there is little research done so far in using Phase Change Material (PCM) fluids and pin fins in microchannels to enhance the heat transfer.

PCM fluids exhibit greater heat transfer when the phase change material undergoes liquid-to-solid transformation. Staggered pins in microchannels have also shown higher heat removal characteristics because of the continuous breaking and formation of the thermal and hydrodynamic boundary layer; they also exhibit higher pressure drop because pins act as flow obstructers.

This paper presents numerical results of circular, square, straight rectangular microchannels with various aspect ratios (1:2, 1:4 and 1:8), and rectangular microchannels with two characteristic staggered pins (square and circular, fixed height with no variation in aspect ratio). The heat transfer performance of a single phase fluid

and PCM fluid in all of these microchannels and the corresponding pressure drop characteristics are also presented.

An effective specific heat capacity model was used to account for the phase change process of PCM fluid. Comparison of heat transfer characteristics of single phase fluid and PCM fluid are presented for all the geometries considered. Among the straight microchannels, 1:8 geometry was found to have the highest Nusselt number. The use of PCM fluid in straight microchannels increased the Nusselt number by 3-7% compared to the single phase fluids. Among the staggered pin microchannels, circular pins were found to be more effective in terms of heat transfer by exhibiting higher Nusselt number. Circular pin microchannels were also found to have lower pressure drop compared to the square pin microchannels. Overall, for all the geometries considered, it was found that the PCM fluid enhances the heat transfer compared to the SPF fluid.

DEDICATION

To my loving and ever supporting parents, sweet sister, and friends for their support and encouragement.

ACKNOWLEDGEMENTS

I would like to express my sincere gratitude to Dr. Jorge L. Alvarado for all the guidance and support he has provided me in the past couple of years. I would not have made so much progress in my research and academics at A&M without his valuable advice. I would like to thank Gurunarayana Ravi for sharing the knowledge that he has accumulated during his research. It is this knowledge that laid a solid basis for my research. I would like to thank my committee members, Dr. Sai Lau and Dr. Hamn-Ching Chen, for their valuable input. I would like to thank the National Science Foundation (NSF) STTR/SBIR program and Dr. Thies of Thies Technology, Inc. for their support.

Finally, I want to thank my parents, Mr. Yadagiri Kondle and Mrs. Bhagyalaxmi Kondle, for their continuous support and encouragement throughout my life. They went through all the hardships to support my higher education. My parents, sister, and friends have always believed in my capabilities and have supported me in every walk of life.

NOMENCLATURE

Variables

c	Volumetric concentration of PCM
c_m	Mass concentration of PCM
C_p	Specific heat of bulk fluid (slurry)
f	Friction factor
h	Convective heat transfer coefficient
k	Thermal conductivity
Z	Distance along the axial direction
$Z+$	Non dimensional distance along the axial direction
L_h	Latent heat of PCM particles
Nu	Nusselt number
p	Pressure
PCM	Phase change material (fluid)
SPF	Single phase fluid
T	Temperature
$\vec{v}$	Velocity
μ	Viscosity
ρ	Density
$(\ )_f$	Property of the carrier fluid
$(\ )_p$	Property of the PCM particle (N-Eicosane)
$(\ )_b$	Property of the bulk fluid (PCM + water)
$\dot{m}$	Mass flow rate of the slurry or fluid

P	Perimeter of the cross section
Pr	Prandtl number
q”	Heat flux
x	Cartesian co-ordinate along x direction
y	Cartesian co-ordinate along y direction
z	Cartesian co-ordinate along z direction

Greek symbols

μ	Dynamic viscosity
ρ	Density

Subscripts

b	Bulk
i	Inlet
w	Wall
1	Start of melting
2	End of melting

Superscripts

``	Flux
-	Average

Acronyms

CHF	Constant heat glux
CWT	Constant wall temperature
PCM	Phase change material

TABLE OF CONTENTS

Page

Page

LIST OF FIGURES

Page

Page

Page

LIST OF TABLES

Page

1. INTRODUCTION

1.1 Microchannels for electronic cooling

Microchannels have been extensively studied for electronic cooling applications because their ability to manage high heat transfer rates compared to conventional channels including ducts and concentric tubes. Heat transfer rate is highest when velocity gradients are significant to ensure proper momentum transport. In microchannels, fluids exhibit high velocity gradients which translate into high heat transfer at the expense of pressure drop. Many microchannel configurations have been studied for their effectiveness in heat transfer applications. Various cross sections like square, rectangular, trapezoidal have been studied extensively. Along with various configurations of microchannels, many fluid phenomena have been researched for their effect on heat transfer removal. Surface roughness, boiling, surface tension effects are some of the phenomena researched for their effect on heat transfer rate.

1.2 Phase change materials

One of the methods to improve the heat transfer is to make use of the latent heat of fusion along with the sensible heating (specific heat) of fluids. The use of latent heat provides for higher storage and transport of heat generated in electronic cooling. In this regard, materials with high latent heat of fusion need to be chosen. Typical phase change

---

This thesis follows the style of *Numerical Heat Transfer, Part A.*

materials (PCM) such as paraffins have the desired high latent heat capacity and hence have the potential to enhance the heat transfer rate. These phase change material fluid particles can be mixed with water to make PCM slurry to be used for electronic cooling. The desirable properties for the particles to make the slurry would be 1) density close to the carrier fluid, 2) high thermal conductivity 3) high heat capacity, and 4) low volume change during phase change process. Some examples of such materials can be paraffins and organic PCMs. For this study, n-Eicosane particles were considered as the Phase Change Material (PCM).

1.3 Motivation for current work

Electronic cooling applications require large heat flux to be removed from small areas. Microchannels have very small volume, high surface-to-volume ratio and large heat transfer coefficients which make them one of the best choices for electronic cooling. However, microchannels have high pressure drop compared to the conventional channels resulting in higher pumping power requirements. Many researchers have tried to increase the heat transfer while lowering the pressure drop by using various geometries and fluids. So far, a lot of progress has been made in the use of single phase fluid in microchannels for achieving enhanced heat transfer. However, extensive literature review shows that not much of information is available in using the PCM fluids, especially at the micro level. Some researchers have studied the PCM fluid characteristics at macro level and in simple geometries like circular and rectangular channels. But, the PCM fluid flow characteristics in the microchannels have not been

studied except very few publications in standard circular and rectangular microchannels. The results from the use of PCM fluids at macro level suggest that they enhance the heat transfer compared to the single phase fluid without much increase in the pressure drop. Hence, it is of interest to study how the PCM fluids affect the heat transfer characteristics in microchannels.

Staggered pins have been used in micro and macro level channels to enhance heat transfer. Having pins in the channels results in continuous breakage and formation of the boundary layer. This continuous breaking of the boundary layer results in larger velocity gradients and hence higher heat transfer. But, having pins in the channel has an undesirable effect on pressure drop. For this reason, different shapes and sizes of microchannels are under study to obtain the most optimal heat transfer performance with the lowest pressure drop possible. Since pins still provide for higher heat transfer, it is important to study how PCM fluids can enhance heat transfer when pins are used.

Experimental studies on microchannels and the use of PCM fluids are time consuming and require lot of effort including the fabrication of micro-scale pins. Numerical analysis is very useful in such cases to determine the effect of pin geometry and pin size on heat transfer. The use of Computational Fluid Dynamics (CFD) reduces cost, time and effort required to understand the flow and heat transfer characteristics of microchannels using PCM fluids. Considering all these factors, PCM fluids seem to be a promising alternative for heat transfer applications in electronic cooling. The study of such fluids in microchannels should shed light on the potential benefits associated with both microchannels with staggered pins and PCM fluids.

1.4 Aim and objectives of current study

First, single phase fluid (water) flow is numerically simulated in straight microchannels with circular and rectangular cross sections with different aspect ratios. Pressure drop and Nusselt number for fully developed flow conditions for these geometries is validated with results available in the literature. Three different boundary conditions, H1 (constant axial heat flux with constant peripheral wall temperature), H2 (constant axial and peripheral heat flux with variable peripheral temperature), T or CWT (constant wall temperature) were considered and the corresponding Nusselt numbers were validated.

Experimental PCM flow performance data for circular ducts is available in the literature. These available experimental results were taken to validate the phase change model used in the simulations. The results from the PCM fluid flow simulations were found to be close to the experimental results.

Once the single phase fluid flow and PCM fluid flow were validated separately, PCM fluid flow simulations were performed for the microchannels for square and rectangular cross sections with various aspect ratios. Three different boundary conditions, mentioned above, were also considered for the PCM fluid flow as well. Staggered pin geometries were also studied for their heat transfer performance using both single phase fluid and PCM fluid. Two characteristic pin shapes, circular and square pins with fixed height (no variation in aspect ratio) were considered. Laminar flow simulations were performed for three different Reynolds numbers for these geometries.

2. LITERATURE REVIEW

In this section, a brief background of related literature is presented. Literature review is divided into three sections. The first section summarizes the findings on the use of microchannels for heat transfer. In the second section, a review of the available literature in the use of PCM fluids at both micro and macro levels is presented. In the third section, research findings from staggered pin channels using various pin cross sections that are available in the literature are summarized.

2.1 Microchannels

To perform numerical simulations in microchannels, it is necessary to know whether the conventional correlations (like Navier-Stokes Equations) used at macro scale are applicable to the microchannels or not. To this extent, Lee et al. [1] have investigated the validity of the conventional correlations of fluid flow and heat transfer at the micro level. They performed numerical and experimental testing of fluid flow characteristics in microchannels of width between 194 μm to 534 μm with water in the Reynolds number range of 300 to 3500. Their results showed good agreement between numerical and experimental findings with an average difference of about 5%. Hence, it can be said from the results by Lee et al. [1] that the conventional correlations for fluid flow and heat transfer are applicable at the micro scale.

Wei et al. [2] performed numerical and experimental study of stacked microchannels. They considered both counter flow and parallel flow arrangements to

obtain temperature uniformity and lower peak temperature. The results showed that the counter flow arrangement results in more temperature uniformity whereas the parallel flow type results in lower peak temperature. Stacked microchannels also resulted in a lower pressure drop.

Lee and Garimella [3] did an extensive study of fluid flow and heat transfer through rectangular microchannels with different aspect ratios, similar to the first step performed in the current study. They considered two boundary conditions (H1 and T) and came up with correlations for Nusselt number based on the channel aspect ratio. Their results were very helpful in knowing the method to simulate H1 condition and validating the Nusselt number for the microchannel aspect ratios considered in this study.

2.2 PCM fluid flow

The characteristics of PCM materials were studied extensively for applications which require heat storage and transport. Since the current study concentrates only on heat transfer and pressure drop, the corresponding literature and the findings so far in this field are presented.

Yamagishi et al. [4] studied the basic characteristics of PCM slurries as heat transfer fluids. They used slurry of water containing $C_{18}H_{36}$ particles with a volume fraction of about 0.3 in their experiments. Their research revealed that the heat transfer coefficient increased for the melting slurry compared to the non-melting slurry. Alvarado et al. [5] presented the physical properties of MPCM slurries in the

temperature range between 2 to 8^{o} C. They measured the heat transfer coefficient, latent heat of fusion, melting and freezing points, and viscosity with respect to temperature and MPCM concentration. Their experimental results suggested that the MPCM behaves as a Newtonian fluid for concentrations below 18.0%.

Chen et al. [6] performed experiments on flow through circular tube under constant heat flux with slurry containing water as carrier fluid and bromohexadecane as PCM particles. Their experiments showed that PCM slurries are very promising alternative as heat transfer fluids compared to water. When the PCM slurry is used, they found that the average wall temperature was lower by 30% and heat transfer enhancement was 1.4 times compared to water. The pressure drop for the same amount of heat transfer was found to be 67% lower using PCM slurry instead of water. Their results were used to validate the phase change model used in the current study.

The specific heat model used to model the phase change process in the current study was developed by Alisetti and Roy [7] based on first principles (i.e. energy balance). Before their model was developed, most of the researchers simulated the PCM flow by using complicated source terms into the energy equation. Instead, Alisetti and Roy [7] developed a simple specific heat model that accounts for the latent heat into the specific heat over the melting range of the PCM particles. They came up with several models with varying approximations and studied those models' effectiveness in estimating the heat transfer accurately. After comparisons of these several models, they suggested that the exact method to account for the latent heat was not very important as long as the melting range and latent heat were taken into account accurately. They

simulated PCM slurry flow in circular duct with constant wall temperature using a specific heat model and found that the model predicts the heat transfer behavior reasonably and accurately. Roy and Avanic [8] later on used the simple linear specific model (used in the current study) to simulate the PCM slurry flow in circular channel with constant heat flux. They showed that the results using the specific heat model are very close to the experimental results.

There are several other studies performed on the heat transfer enhancement using PCM slurry flows. Wang et al. [9] experimentally investigated the PCM fluid flow characteristics for various concentrations of PCM ranging 5% to 27.6%. However, there are very few publications in which PCM flow is studied in microchannels. Hao and Tao [10] developed a numerical model and did an extensive study on PCM slurry flow through circular microchannel under constant heat flux condition. Their results are significant because they solved the particle motion independent of the fluid motion using separate momentum equations. They also considered the effects of particle-depleted layer, particle-wall interaction, inter-particle interaction along with solving separate mass, momentum and energy equations. Solving for separate equations considers the fact that, the fluid velocity and temperature would be different from that of the particle velocity and temperature. Sabbah et al. [11] considered 3-D conjugate heat transfer through microchannels with PCM slurry. Their results showed that lower and more uniform wall temperature could be obtained in the case of PCM slurry compared with water as heat transfer fluid.

Ravi et al. [12] numerically studied the performance of PCM slurry flow in finned tubes. They found that the specific heat model gave good results that are comparable with available literature. They presented the results using the PCM fluid for different fin heights, and different boundary conditions (H1 and T). The study showed that the PCM fluid significantly enhances heat transfer in finned tubes.

A thorough literature review suggests that not much of research has been done in the use of PCM fluids in microchannels. However, at a macro scale, good amount of data is available in the literature on the PCM performance as heat transfer fluid. Hence, this study is very important and complements the available literature on PCM fluid flow particularly in microchannels.

2.3 Use of pins to enhance the heat transfer

Fin-pins enhance heat transfer because of the continuous breakage and formation of the boundary layer. However, pressure drop would be higher in the presence of pins resulting in increased pumping power. Several studies have been performed on the use of pins in channels with the goal of increasing the heat transfer without increasing pressure drop.

Prasher et al. [13] studied the flow and thermal performance of square and circular pins on a cold plate under cross flow. They used water as the heat transfer fluid and found that the Nusselt number varies as a function of $Re^{0.85}$ for Reynolds number below 100, and $Re^{0.73}$ for Reynolds number greater than 100. Kosar et al. [14] did experimental investigation of flow and heat transfer over a bank of micro pin-fins. Their

studies suggested that there exists significant discrepancy between several different correlations available on bank of pin-fins. These discrepancies are in the range of about 30%, making it difficult to choose any given correlation as a standard at the micro-scale.

There are relatively less numerical studies, compared to experimental studies, on the use of pins for heat transfer enhancement. Part of the reason being that is complex and computationally expensive to numerically study such type of geometries. However, Agaro and Comini [15] developed their own numerical model to analyze the heat transfer characteristics of pins of three different cross sections, square, circular and elliptical. They simplified the geometry by considering only a set of pins that are characteristic to the geometry and used periodic boundary conditions to analyze the fully developed flow characteristics. However, it does not address the effect of pin spacing on heat transfer.

3. METHODOLOGY

3.1 Background

This section provides the basic equations, assumptions, properties and specific heat model used in the current study.

3.1.1 Governing equations

The basic equations to solve the fluid motion and the heat transfer are mass conservation (Continuity), momentum conservation (Navier-Stokes) and energy equation. These basic equations [16] are listed below:

$$\nabla \cdot (\vec{v}) = 0 \tag{1}$$

$$\nabla \cdot (\rho \vec{v} \vec{v}) = -\nabla p + \nabla \cdot (\bar{\bar{\tau}}) \tag{2}$$

$$\nabla \cdot \left(\vec{v}(\rho E + p)\right) = k \nabla \cdot \nabla T + \nabla \cdot (\bar{\bar{\tau}} \cdot \vec{v}) \tag{3}$$

These equations do not have a direct analytical solution except for very simple cases, and hence have to be solved in the discretized form in a domain. In this study, they are solved using finite volume technique using commercial computational fluid dynamics (CFD) software GAMBIT and FLUENT.

3.1.2 Assumptions

Basic assumptions taken in this study are listed below. They are valid for both single phase fluid and PCM fluid flow.

a. Fluid continuum is assumed in microchannel flow.

b. Fluid is assumed to be Newtonian.
c. Incompressible flow.
d. Surface is considered to be smooth and no-slip condition is used on all wall surfaces.
e. Fluid properties are assumed to be constant with respect to temperature.
f. Buoyancy effects are neglected as density is assumed to be constant.
g. Natural convection effects are neglected.

Apart from the basic assumptions for the fluid flow, certain assumptions are made to model the phase change process. These assumptions are listed below.

a. The fluid-particle nature of PCM slurries was simplified by assuming a homogenous liquid with physical properties that are based on the concentration of PCM.
b. No volume change is assumed during the phase change process.
c. Inter-particle interaction and particle-wall interactions are neglected.
d. Phase change process is assumed to take place within a specific temperature range.
e. Phase change process is approximated using a specific heat model.

3.1.3 Specific heat model

It is difficult to model the entire phase change process and particle flow as it happens in reality without making use of the assumptions listed above. A thorough review of literature suggested that except for the work by Hao and Tao [10] and Xing et

al. [17], no other study considered particle-particle interactions, non thermal equilibrium and other complexities involved in PCM slurry flow. Most of the studies on PCM slurry flow used approximate models to take account of latent heat assuming thermal equilibrium between fluid and particles, as observed by Ravi et al. [12].

One of the methods used to consider the latent heat is to include a heat source (sink) term in the energy equation, equal to the latent heat of the PCM material. This was first suggested by Charunyakorn et al. [18]. Though this method is a good approximation and gave reasonably accurate results, it is relatively complex compared to the models developed later on by other researchers.

Alisetti and Roy et al. [7] came up with very simple and approximate models that account for the phase change process. They started with a hypothesis that the latent heat can be accounted for by changing the specific heat within the melting range. First, one needs to know and assume a melting range (MR), which is the temperature range between when PCM starts and ends the melting process. For temperatures below and above the melting range, the specific heat of the slurry is a simple weighted average of the specific heats of the fluid and the PCM, the weights being the mass concentrations. For temperatures in between the melting range, specific heat is the weighted average of fluid specific heat and the corresponding effective specific heat of the PCM material based on its latent heat. This effective specific heat is obtained using the latent heat and the melting range. The specific heat can be assumed to vary using different functions (like sine curve, left rectangle, etc.) during the melting range to account for the heat release (latent heat) during the phase change process. However, after considering all

these various methods, it is found that all of them give same results in terms of heat transfer. Hence, it is of advantage to use the simplest model for numerical analysis. This model is summarized in the following equations,

The melting range is between temperatures T_1 and T_2,

For $T < T_1$ or $T > T_2$ [8]:

$$C_{p,b} = c_m \cdot C_{p,p} + (1 - c_m) \cdot C_{p,f} \tag{4}$$

For $T_1 < T < T_2$ [8]:

$$C_{p,b} = (1 - c_m) \cdot C_{p,f} + \frac{c_m \cdot L_h}{(T_2 - T_1)} \tag{5}$$

The specific heat versus temperature and enthalpy versus temperature plots given in Figure 1 and Figure 2 provide a better picture of how the change in specific heat affects the fluid heat transfer capacity.

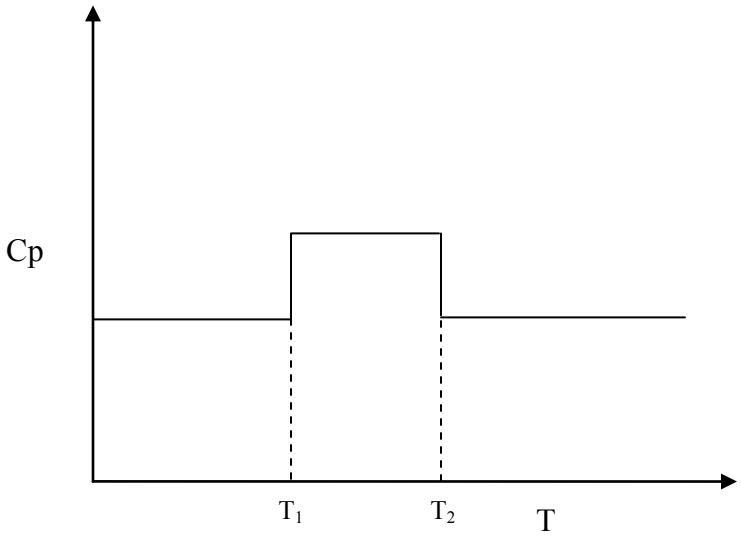

Figure 1 Specific heat variation with temperature

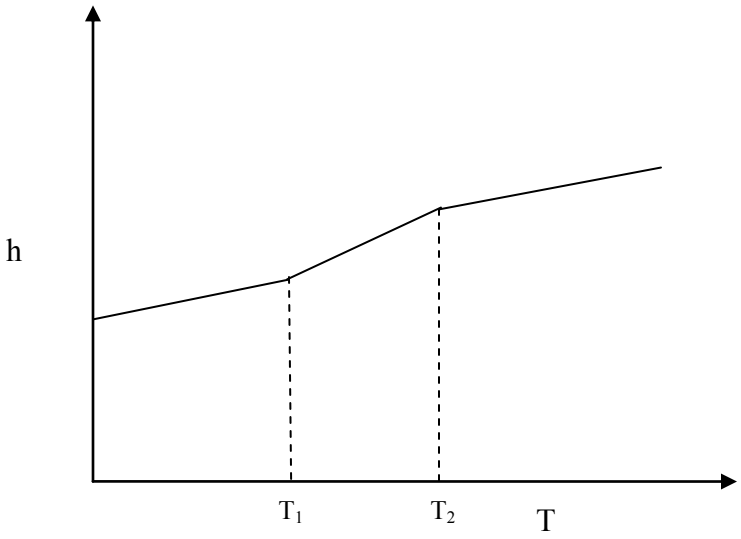

Figure 2 Enthalpy variation with temperature

3.1.4 Explanation of thermal boundary conditions

There are two main types of thermal boundary conditions that can be applied at the wall. One is specifying a constant heat flux and the other is specifying a constant

wall temperature. Also, there are two different ways of specifying constant heat flux. These boundary conditions are listed and explained below:

i. Constant axial heat flux with constant peripheral wall temperature (H1)

ii. Constant axial and peripheral heat flux (H2)

iii. Constant wall temperature (T)

The constant wall temperature condition is easy to apply. The applications in which such a boundary condition is used would be condensation, evaporation, and other processes where the heat exchanger wall temperature almost remains constant. In this case, the heat flux from the wall to the fluid is not known and need to be calculated from the fluid flow solution.

The constant heat flux boundary condition has two variations, H1 and H2. In the case of H1 condition, the heat flux is constant in the axial direction and the temperature is held constant in the peripheral (angular) direction. The H1 boundary condition is more reasonable, practical and considers the actual physics of most heat transfer phenomena [19]. It has been found in majority of the studies that H1 condition is more appropriate and close to the experimental findings than H2 condition. In the case of H2 boundary condition, both the axial and peripheral heat flux is held constant and hence peripheral wall temperature varies. This type of boundary condition is widely used in numerical studies for its modeling simplicity, but it does not have much practical importance as majority of the heat exchangers fall into either H1 or T boundary conditions. It is important to note that H1 and H2 difference occurs only when the solid wall thickness is assumed to be zero. When the wall thickness is considered, as in the

case of conjugate heat transfer problems, H1 and H2 does not make any difference as the heat transfer inside the solid is modeled and the heat flux is applied at the bottom wall, away from the fluid-solid interface. For the staggered pin microchannels, conjugate heat transfer is modeled and hence H1 and H2 does not make any difference, and the boundary condition is simply termed as constant heat flux (CHF) for those geometries. Another exception is the case of circular duct and channel with zero wall thickness, where both the heat flux and wall temperature remain constant in the peripheral direction because of symmetric geometry.

3.2 Fluid properties and flow parameters

This section explains the fluid properties, calculation of the PCM slurry properties, flow parameters used and how they were calculated.

3.2.1 Fluid properties

In this study, water and n-Eicosane were used as the carrier and PCM, respectively. A volume concentration of PCM of 15% was considered for all the simulations. The slurry properties were based on this volumetric concentration, and were calculated using correlations available in literature. The exact melting temperature of n-Eicosane is 310K, but a melting range of 309-310 K was assumed for numerical stability. The latent heat of n-Eicosane is 230kJ/kg. The equations used for calculation of PCM slurry properties are given below. From here on, the properties of the slurry are called as “bulk-fluid” properties.

Viscosity [11]:

$$\frac{\mu_b}{\mu_f} = (1 - c - 1.16c^2)^{-2.5} \tag{6}$$

Density [11]:

$$\rho_b = c \cdot \rho_p + (1 - c) \cdot \rho_f \tag{7}$$

Thermal Conductivity [11]:

$$k_b = k_f \cdot \frac{2 + {k_p}/{k_f} + 2c\left({k_p}/{k_f} - 1\right)}{2 + {k_p}/{k_f} - c\left({k_p}/{k_f} - 1\right)} \tag{8}$$

In the above equations, μ stands for viscosity, ρ stands for density and k stands for thermal conductivity. The subscripts b, f and p stand for bulk, fluid and particle (PCM), respectively.

Specific heat was calculated using Equation (1) and Equation (2) depending upon the temperature. The properties of fluid and PCM particles used, and the resulting slurry properties are given in Table 1 below. The specific heat for the slurry mentioned in the table is the value used for temperatures before and above the melting range of temperature.

Table 1 Particle and fluid properties

Fluid	k (W/m-K)	Viscosity (N-s/m^2)	Density (kg/m^3)	C_p (kJ/kg-K)
Water	0.613	0.000855	997	4.179
PCM	0.15	solid particle	946.4	1.973
Slurry (bulk homogeneous fluid)	0.5246	0.001388	989.41	3.862

3.2.2 Flow and heat transfer parameters

Flow and heat transfer characteristics are generally specified using a set of dimensionless numbers. These dimensionless numbers were calculated in different ways, depending upon the geometry and the flow conditions. The flow parameters used and the ways they were calculated are explained in this section.

Hydraulic diameter

Hydraulic diameter is the characteristic length used for determining the flow characteristics. It is defined as the ratio of four times the cross-sectional area (perpendicular to the flow) to the wetted perimeter. When using a straight channel, there is no ambiguity in using this formula, but when pins are present in the microchannel, there are two choices when considering the corresponding area and wetted perimeter. One is the channel cross sectional area and the other is the pin cross sectional area. When using pins, it is considered that the pin cross sectional area and perimeter are the characteristic lengths for estimating flow behavior as it is routinely done in banks of

tubes heat transfer problems. For determining hydraulic diameter based on pin cross-sectional area, the following equation is used:

D_{hp} = Pin hydraulic diameter, based on pin cross section given by,

$$D_{hp} = \frac{4A_p}{P_p} \tag{9}$$

$4A_p$ = Area of pin cross section

P_p = Perimeter of pin cross section

For determining hydraulic diameter based on microchannel inlet cross-sectional area, the following equation is used:

D_{hi} = Inlet hydraulic diameter, based on inlet cross section given by,

$$D_{hi} = \frac{4A_i}{P_i} \tag{10}$$

A_i = Area of inlet cross section

P_i = Perimeter of inlet cross section

In this study, both hydraulic diameters were used. These two different methods are differentiated using the subscripts “i” for inlet or fluid cross section based and “p” for pin cross section based.

Reynolds number

Reynolds number is generally used to determine whether the flow is laminar or turbulent. In this study, Reynolds numbers were taken such that the flow remains laminar for the geometries considered. Reynolds number (Re) were calculated based on pin and microchannel hydraulic diameters using the equation given below,

$$Re_p = \frac{\rho V D_{hp}}{\mu} \tag{11}$$

$$Re_i = \frac{\rho V D_{hi}}{\mu} \tag{12}$$

In the above equations, V is the average velocity at the inlet of the channel. For the case of microchannels with pins, this velocity is also equal to the maximum average velocity inside the channel as used by Incropera and Dewitt [20]. Other properties like density and viscosity are taken from the fluid properties, which in this study is the PCM slurry.

Prandtl number

Prandtl number is the ratio of momentum to thermal diffusivity [20]. It represents the relation between thermal boundary layer and momentum boundary layer. In this study, it is used to calculate the non-dimensional distance.

$$Pr = \frac{C_{p,b} \cdot \mu_b}{k_b} \tag{13}$$

Non-dimensional distance

The non-dimensional distance represents the characteristic length for many heat transfer applications. In the case of microchannels, the non-dimensional distance is used to determine when the flow becomes fully developed. In laminar and turbulent flow, it is possible to specify a non-dimensional distance (Z^+) after which the flow will be fully developed, for a specific geometric shape based on the Reynolds number. All the heat transfer variables presented in the study are plotted against the non-dimensional distance.

$$z^+ = \frac{z}{r \cdot Re \cdot Pr} \tag{14}$$

where,

$$r = {D_h}/{2} \tag{15}$$

Any of the two hydraulic diameters (Equations 9 and 10) can be used to calculate r. The choice of the hydraulic diameter is based on the variable plotted against the dimensionless distance. For example, when Nusselt number is calculated on the basis of inlet hydraulic diameter, non-dimensional distance is also calculated using the inlet hydraulic diameter when plotting Nu versus Z^+.

Friction factor

Friction factor is a dimensionless number that accounts for pressure drop (friction) in fluid flow. The friction factor for a specific geometric shape can be specified

as a function of Reynolds number for laminar flow in straight sections. In this study, the fanning friction factor was used, which is given by,

$$f = \frac{D_{hi} \cdot \Delta p}{2L\rho V^2} \tag{16}$$

Fluid bulk temperature

Bulk temperature of the fluid is the mass weighted average temperature of the fluid at a given cross section in the channel. Among the different ways of calculating the average fluid temperature like area-weighted, facet average etc., mass weighted average gives the best estimate (from energy balance) . Mass weighted average is calculated based on the following equation,

$$T_b = \frac{\sum_{i=1}^{n} T_i \rho_i \left|\vec{v}_i \cdot \vec{A}_i\right|}{\sum_{i=1}^{n} \rho_i \left|\vec{v}_i \cdot \vec{A}_i\right|} \tag{17}$$

Heat transfer coefficient

The convective heat transfer coefficient is calculated based on the average fluid and wall temperatures at a given location. The average heat flux from the wall is known from the simulation and this is used to calculate the heat transfer coefficient, given by the equation,

$$h = \frac{q''}{(T_w - T_b)} \tag{18}$$

q'' = Average wall heat flux along the periphery at a particular axial location

T_w = Average wall temperature along the periphery at a particular axial location

T_b = Mass weighted average of fluid temperature on the cross section at a particular axial location

For the constant heat flux boundary condition, q'' is known since it is one the input variables, but T_w needs to be calculated from the simulation. For the case of constant wall temperature, T_w is known whereas q'' needs to be calculated from the simulation. Whether it is T_w or q'' that needs to be determined from the simulation, both are calculated in the same way by taking the average value along the periphery of the wall. For straight microchannels (without pins) it is easy to calculate wall temperature when imposing H1 or H2 boundary conditions or heat flux when imposing CWT boundary condition. However, in the case of staggered pin microchannels where heat transfer boundary conditions are only applied at the bottom surface, the average surface temperature or heat flux required for heat transfer coefficient calculations was determined at the midpoint of every pin as shown in Figure 3. This allowed for consistent calculation of wall temperatures despite the changes in the wall surface topology along the flow direction (because of pins). The first five axial locations where these values were calculated are shown as lines in Figure 3. At each of these locations, a line is drawn that represents the fluid-solid interface at that location. The average heat flux or the average wall temperature can be calculated by taking the corresponding average values along this line. A detailed description of microchannel geometries used in the study is presented in the section 3.3.1.

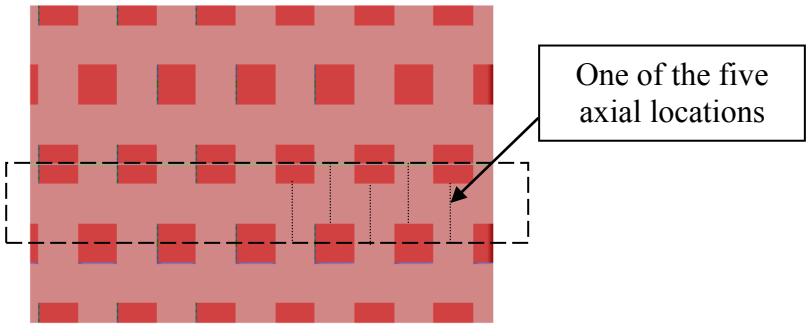

Figure 3 Square pins geometry showing the locations used for calculation

Nusselt number

Nusselt number is one of the very important parameters for analyzing heat transfer performance. Higher the Nusselt number, more effective is the heat transfer process. This dimensionless number essentially indicates the effectiveness of the convective heat transfer process taking place between the walls and the fluid. It is based on the convective heat transfer coefficient and is given by,

$$Nu_p = \frac{hD_{hp}}{k_b} \tag{19}$$

$$Nu_i = \frac{hD_{hi}}{k_b} \tag{20}$$

where,

Nu_p = Nusselt number based on pin hydraulic diameter

Nu_i = Nusselt number based on inlet hydraulic diameter

The only difference between the above two Nusselt numbers is the hydraulic diameter used for calculation.

3.3 Modeling procedure

Heat transfer and fluid simulations of laminar flow in microchannels were performed using computational fluid dynamics (CFD) software Gambit and Fluent. The geometry and grid of interest were created in Gambit. The flow and heat transfer simulations were performed using Fluent. The steps followed for the entire modeling are shown in Figure 4.

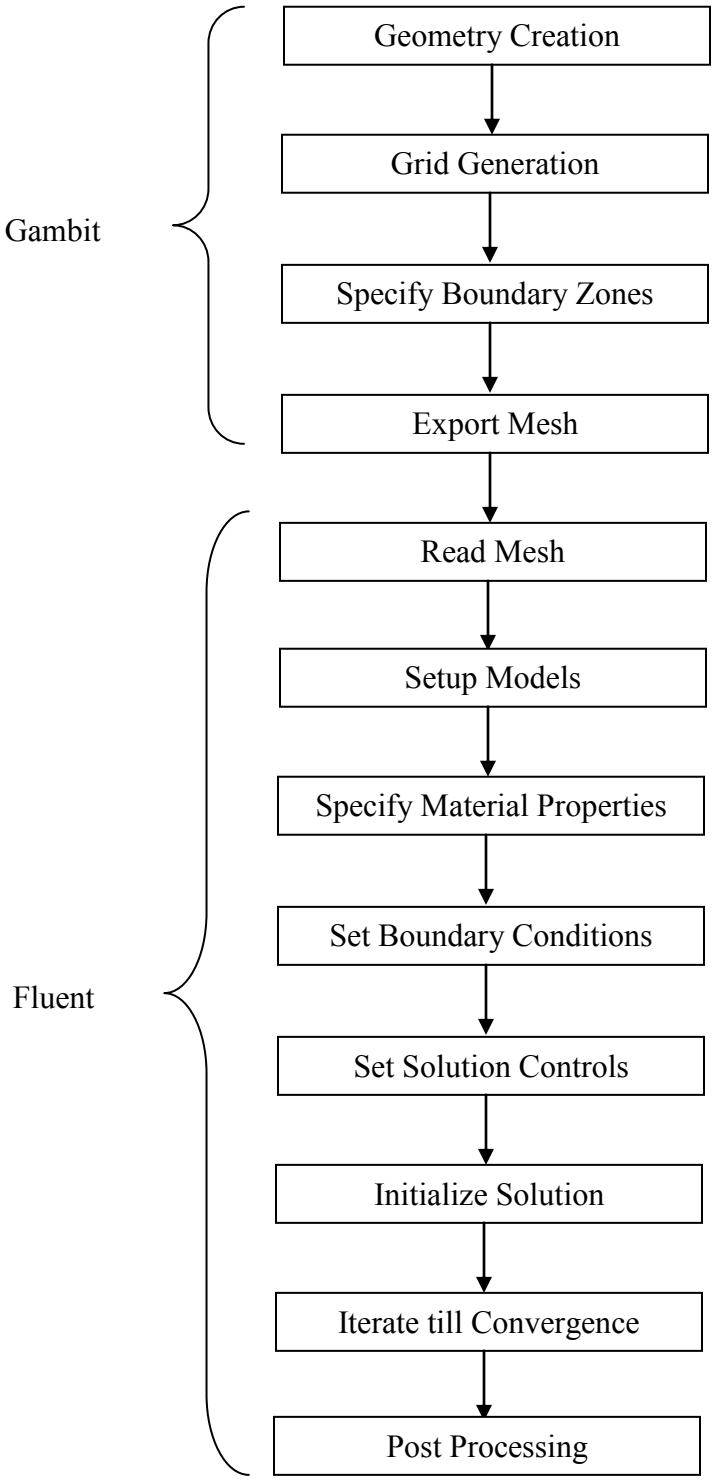

Figure 4 Steps followed for simulation

3.3.1 Geometry and grid

First, circular and rectangular microchannels with three different aspect ratios with no pins were considered in the study to determine the effect of cross-sectional shape on Nusselt and pressure drop. The difference between the rectangular microchannels is the difference in aspect ratio of the cross section including aspect ratios of 1:2, 1:4 and 1:8 as shown in Figure 5.

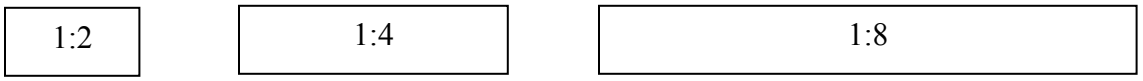

Figure 5 Three geometric aspect ratios considered

The dimensions of these channels are given in Table 2. The length of the channels were specified such that the flow could be hydrodynamically and thermally fully developed before the fluid exited the channel. Since these geometries are symmetric, only a quarter of the geometry was modeled using symmetry boundary conditions as shown in Figure 6. The actual cross section and the portion of the geometry modeled are given below.

Table 2 Dimensions of microchannels modeled

Dimension	Geometry		
	1:2	1:4	1:8
Height (μm)	150	150	150
Width (μm)	300	600	1200

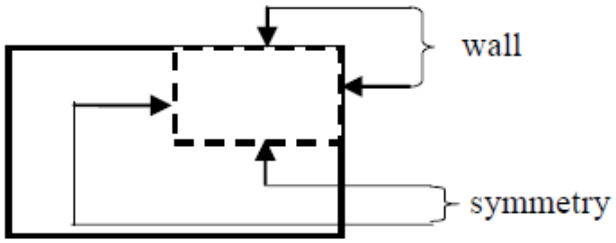

Figure 6 Cross section showing the portion modeled

Once the single phase and PCM fluid flow results were obtained for the above microchannels, microchannels with staggered pins were considered. When pins were used, a thick bottom wall was added to provide support for the pins. By adding a thickness to the wall and applying heat transfer boundary conditions at that bottom surface only, the heat transfer simulation became a conjugate heat transfer problem. When conjugate heat transfer is considered, heat transfer equations are solved in the solid domain as well. Two types of pin cross sections including circular and square were considered to understand and measure the heat transfer enhancement caused by pins. It should be noted that three aspect ratios were considered only in the case of straight microchannels. For the case of staggered pin geometries, the pin height is fixed and hence the aspect ratio was fixed. Three different microchannel geometries were considered and were differentiated with the terms “square pins”, “circular pins” and “no-pins.” Considering symmetry, only a portion of these microchannel geometries were numerically simulated in Fluent. The sections modeled are shown in Figure 7 to Figure 11, and the dimensions are listed in Table 3.

From Figure 8 it can be said that the pin arrangement looks similar to an in-line arrangement. This is because the transverse spacing between the pins (S_T = 400 µm) is much larger than the spacing in the flow direction (S_L = 100 µm).Furthermore, the parallel faces of the pins are aligned in the flow direction which is beneficial from the pressure drop standpoint. However, it remains to be seen if a fully staggered pin configuration (i.e. pin faces orthogonal to flow direction) result in much greater heat transfer without incurring in considerably higher pressure drop penalty.

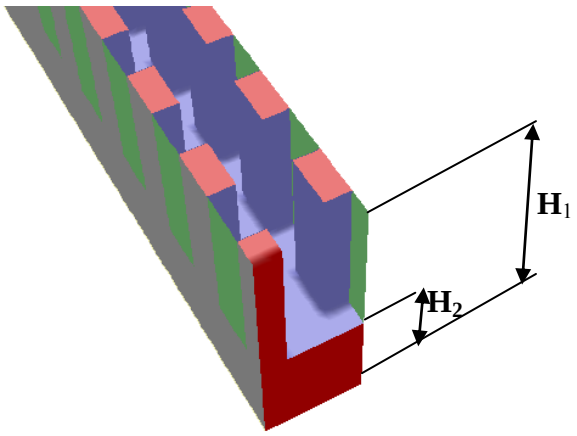

Figure 7 Square pins geometry modeled using symmetry

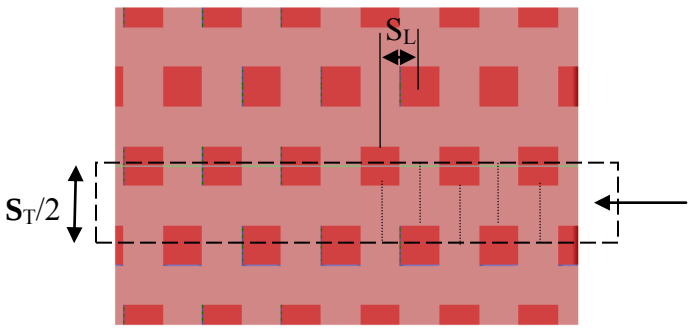

Figure 8 Square pins actual geometry and the portion modeled

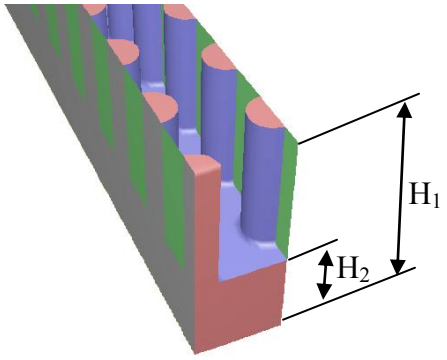

Figure 9 Circular pins geometry modeled using symmetry

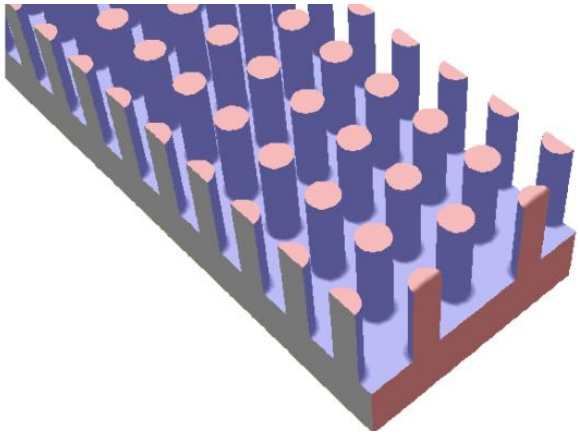

Figure 10 3D view of the actual circular pin channel

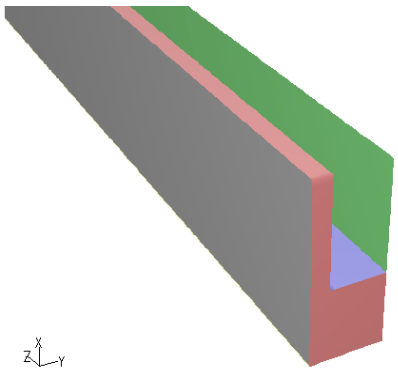

Figure 11 No pins geometry modeled using symmetry

Table 3 Dimensions of staggered pin microchannels

Variable	Description	Dimension (μm)
H_1	Height of entire domain	500
H_2	Height of solid domain	200
S_L	Streamwise Pitch	100
S_T	Transverse Pitch	400
D	Diameter of circular pins	100
L	Side of square pins	100

Once the geometries were created, the corresponding grids were generated consisting entirely of hexahedral elements. Three different grid resolutions were considered to obtain grid independent solution. For microchannels with three different aspect ratios, grids with elements 10x20x100, 15x30x1000 and 15x30x1500 were considered. For the microchannels with pins, 38x13x1400, 43x13x1400, and 42x16x1634 grid elements were numerically simulated, and the results were analyzed.

Grid convergence results are presented in the Results and Discussion section. Figure 12 shows a typical grid near the inlet section.

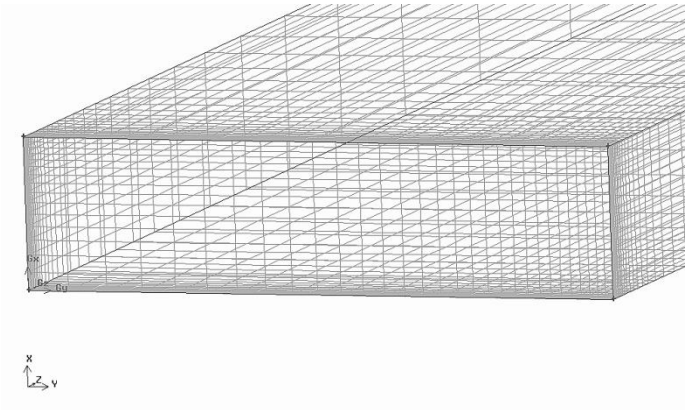

Figure 12 Typical grid near the microchannel inlet

3.3.2 Solving in FLUENT 6.3

Once the required grid was generated, it was exported from Gambit and read by Fluent. Scaling was performed if the geometry and grid were generated in different units. Fluent solution options such as "laminar flow", "steady flow", "turning on energy equation" were set. Material properties were set as calculated for the PCM slurry.

First, velocity at the inlet was set as constant with uniform flow as initial condition. A fully developed velocity profile was obtained for each given microchannel geometry without solving for the heat transfer. Once the velocity profile was obtained, it was used as the inlet boundary condition. Temperature at the inlet was set to 300 K. The fluid pressure at the outlet was set to 1 Atm. Fluent uses this back pressure to calculate the inlet pressure, so that the required mass flow rate (velocity) based on continuity and

momentum could be obtained. Walls were set to non-slip condition. The wall thermal boundary condition was specified as either constant heat flux or constant wall temperature. In the case of constant heat flux, two types of boundary conditions, H1 and H2 were considered. Setting the H2 boundary condition was simply done by specifying the required heat flux. However, setting the H1 boundary condition was difficult, because most of the commercial CFD solvers do not have this condition available in their software package. Lee and Garimella [3] explained how this condition can be set in Fluent using a "thin wall" model with "shell conduction". "Thin wall" model requires the user to set a small thickness (can be very small) to allow for peripheral heat conduction. Setting the "shell conduction" model ensures that the applied heat flux redistributes inside the wall in the peripheral direction. This redistribution of heat flux allows for temperature uniformity in the peripheral direction, resulting in the required H1 boundary condition. It is to be noted that in this case, the heat flux varies in the peripheral direction as opposed to being constant, as in the case of H2 boundary condition.

Flow was simulated using second order accuracy. Continuity, x, y and z momentum equations, and energy equation residuals were monitored. The convergence criterion was set to 10^{-6} for all these equations. Under-relaxation factors within the range of 0.3 to 1.0 were used and were found to give good convergence behavior and accurate results. Apart from checking residuals for convergence, velocity and temperature at specific locations inside the geometry were monitored and made sure that they reach constant values (with no variation for further iterations).

4. RESULTS AND DISCUSSION

4.1 Validation

It is very important to validate the simulation methodology. Many lessons were learnt during the validation process, especially in the application of boundary conditions and extracting (post processing) the results from the simulation. Since velocity was the input for these simulations, it was necessary to validate the resulting pressure drop results. For validating the numerical heat transfer results, the theoretical or experimental Nusselt numbers values (available in the literature) were compared with the results from the simulation. Finally, since phase change materials were simulated, it was important to validate the phase change process as well.

This section is divided into two parts, first one showing the validation for the single phase fluid, and the second one showing the validation for the PCM fluid flow.

4.1.1 Single phase fluid (SPF)

Pressure drop can be validated by comparing the friction factors for the geometries considered. Fully developed flow friction factors for rectangular channels of different aspect ratios have already been reported by Kays [21]. The values of f^*Re were compared with those given by Kays [21] and are summarized in Table 4. The Reynolds number used for all the straight microchannels simulations was 700.

To validate the heat transfer, Nusselt number values were also compared for thermally fully developed flow condition. Nusselt number depends on the thermal

boundary condition applied at the wall, and hence should be different. The results for all the three boundary conditions were validated and are summarized in Table 5 to Table 7.

Table 4 Friction factor (pressure drop) validation

Geometry	f^*Re_i – current simulation	f^*Re_i – literature [21]
Circular	16	16
1:2	15.5	15.6
1:4	18.1	18.3
1:8	20.6	20.7

Table 5 Nusselt number validation for T boundary condition

Geometry	Nu – Simulation	Nu– literature [21]
Circular	3.67	3.66
1:2	3.39	3.39
1:4	4.45	4.44
1:8	5.62	5.95

Table 6 Nusselt number validation for H1 boundary condition

Geometry	Nu – Simulation	Nu– literature [21]
Circular	4.40	4.36
1:2	4.1	4.11
1:4	5.29	5.35
1:8	6.41	6.6

Table 7 Nusselt number validation for H2 boundary condition

Geometry	Nu – Simulation	Nu-literature [22]
1:2	3.02	3.07
1:4	2.94	3.03
1:8	2.94	3.03

It can be observed from the above tables that the numerical results match well with the values reported in the literature. Note that as mentioned before, for the circular channel, there is no difference between H1 and H2 boundary condition and hence the Nusselt number would be the same. Also, it can be observed that the Nusselt number for the H2 boundary condition is almost same for all the three aspect ratios considered. This is because the Nusselt number reaches a constant value beyond certain aspect ratios according to Equation (21) for thermally fully developed flow Nusselt number under H2 condition [22]. From the equation, it can be found that the Nusselt number varies significantly for aspect ratios between 0.5 and 1, but for aspect ratios below 0.5, which is the case in current study, it remains between 2.8 and 3.4.

Nusselt number for H2 boundary condition [22]:

$$Nu_{H2} = 8.235(1 - 10.6044\alpha + 61.1755\alpha^2 - 155.1803\alpha^3 + 176.9203\alpha^4 - 72.9236\alpha^5) \quad (21)$$

where,

α =Ratio of the cross section dimensions (height/width)

4.1.2 Phase change material (PCM) fluid

Since the phase change process was accurately approximated with a specific heat model, it is important to validate the results obtained using the model. Chen et al. [6] conducted experiments on PCM fluid flow in a circular channel under constant heat flux condition. The Nusselt number from their experimental results is compared with the values from the simulation as shown in Figure 13.

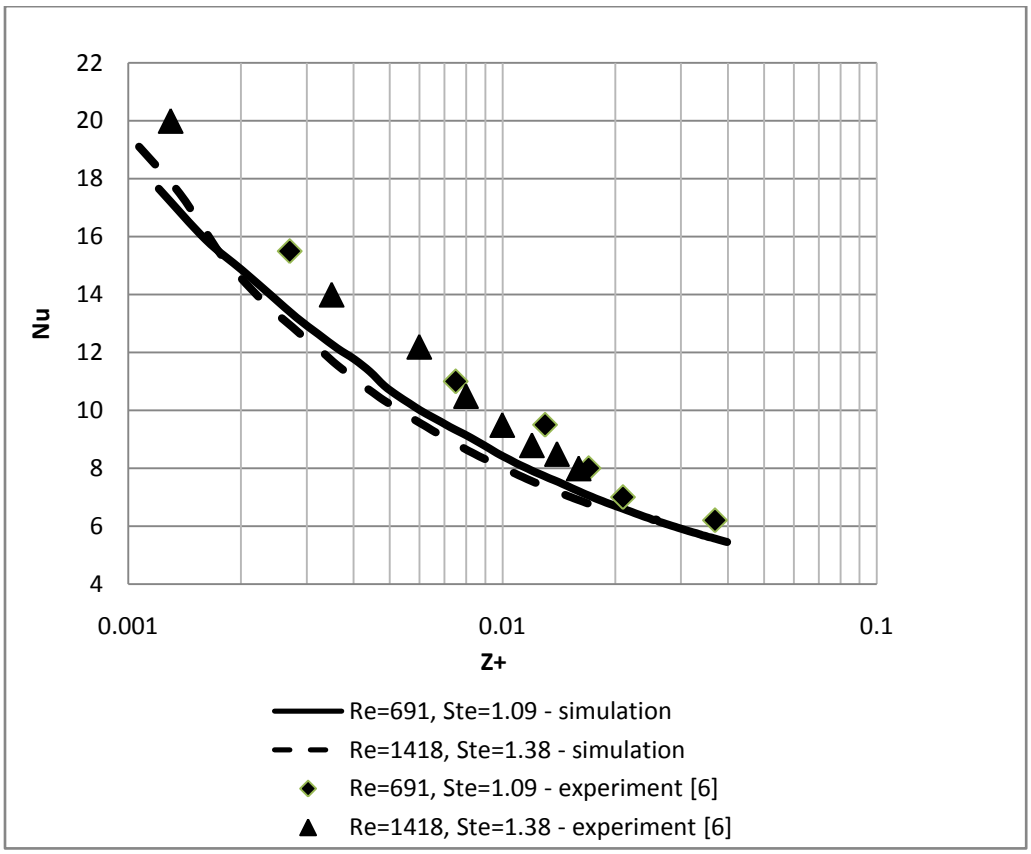

Figure 13 Nusselt number validation for the PCM fluid flow

Since the results are for a circular channel, there is no difference between H1 and H2 boundary condition. The difference in the results is about 15%, and this difference might be due to the difference in calculation procedures and the associated experimental error. Chen et al. [6] calculated the bulk temperature assuming that all the PCM starts melting at a particular axial location (independent of the radial direction) and ends at another axial location. However, in the current study, this assumption is not made as the temperature at any location is known from the numerical simulation. In fact, phase change does not start at the same distance for all fluid particles. The fluid particles closer to the surface experience phase change sooner. From Figure 13, it can be observed from the comparison that the numerical model used for phase change process gives reasonably accurate results.

4.2 Grid independence

Results from a CFD analysis depend initially on the grid resolution, but beyond a particular grid resolution, there would not be much difference in the results. It is this limiting grid that needs to be used since it provides accurate results with the lowest possible computational time (size of the grid).

For the straight microchannels three different grid resolutions were considered with varying resolutions in three directions, 10x20x1000, 15x30x1000 and 15x30x1500. The results from using these grids differed only by about 2%. Both single phase fluid and PCM fluid were simulated and checked for grid independence. Figure 14 shows results of the single phase fluid under H2 boundary condition in a 1:2 microchannel.

Figure 15 shows results for the PCM fluid under H1 boundary condition in a 1:4 microchannel. In both Figure 14 and Figure 15, the results using different grid almost coincide and hence it is difficult to distinguish between the different curves in the plots. The results shown are for Reynolds number of 700.

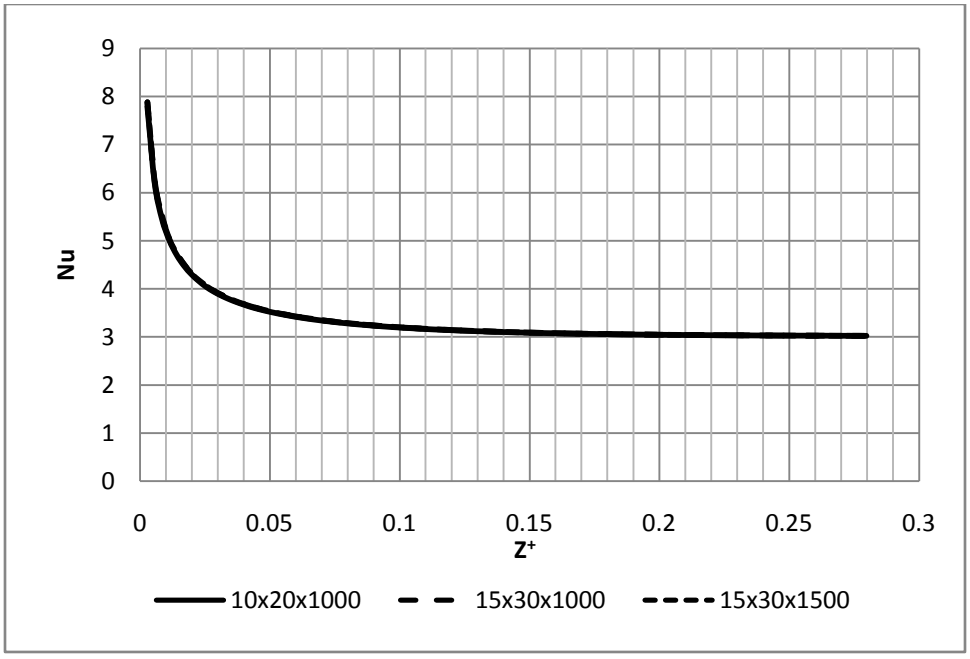

Figure 14 Grid independence using SPF under H2 boundary condition

For the staggered pin microchannels, three grids with resolutions 38x13x1400, 43x13x1400, and 42x16x1634 were considered. The results using these grids varied within 4%. Hence, 38x13x1400 grid was enough to get reasonably accurate results as shown in Figure 16. The results shown in Figure 16 are for the square-pin geometry under CHF boundary condition for a pin Reynolds number (Re_p) of 50.

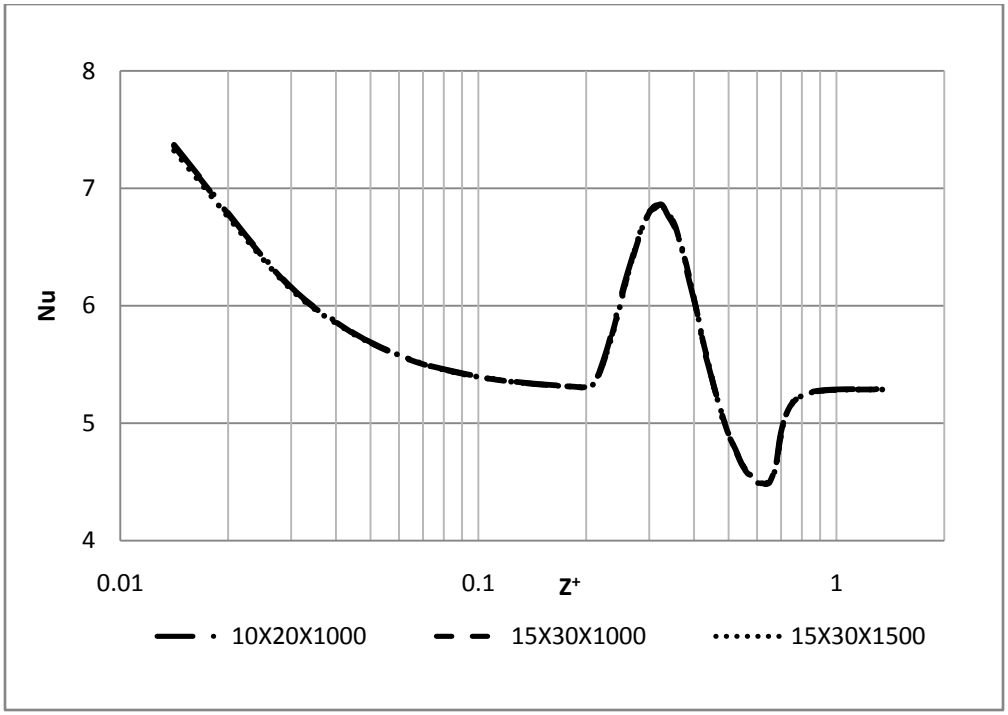

Figure 15 Grid independence using PCM fluid under H1 boundary condition

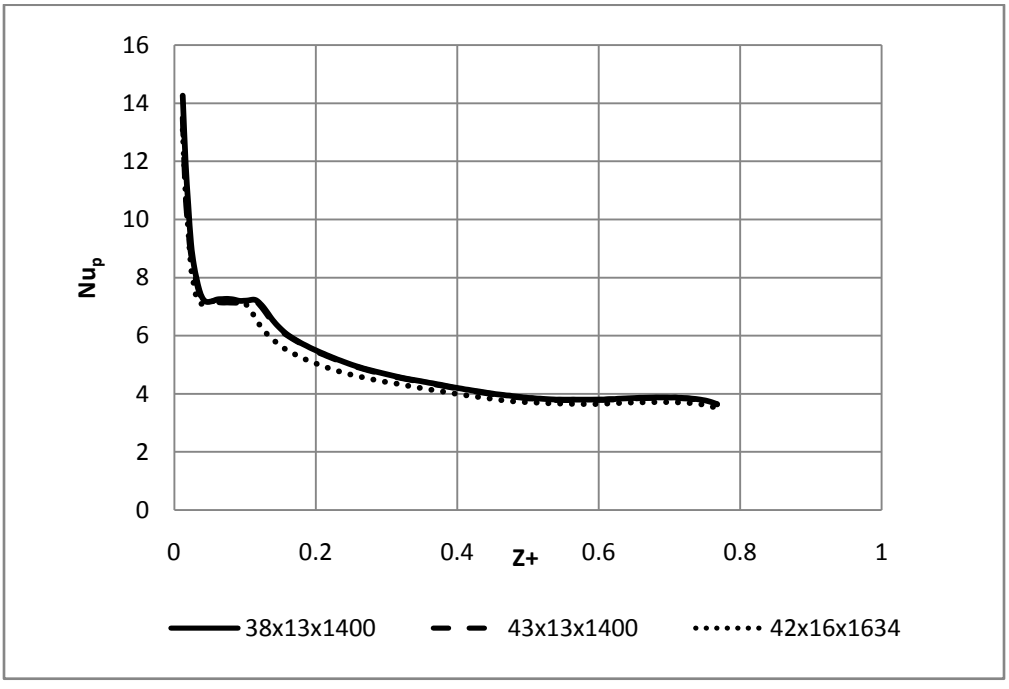

Figure 16 Grid independence using PCM fluid in staggered pin microchannel

4.3 Results using straight microchannels

Results are divided into two sections, first one for straight microchannels with different aspect ratios, and the second one for microchannels with staggered pins. This section presents the results from various simulations performed for the straight microchannels. A Reynolds number of 700 was used for all the simulations. First, only the flow was obtained by solving the numerical problem without applying heat transfer to obtain the fully developed flow velocity profile. The velocity profiles obtained for the three aspect ratios 1:2, 1:4 and 1:8 are shown below in Figure 17 to Figure 19. Each fully developed velocity profile was used as the inlet boundary condition. The results are divided into three subsections based on the thermal boundary condition.

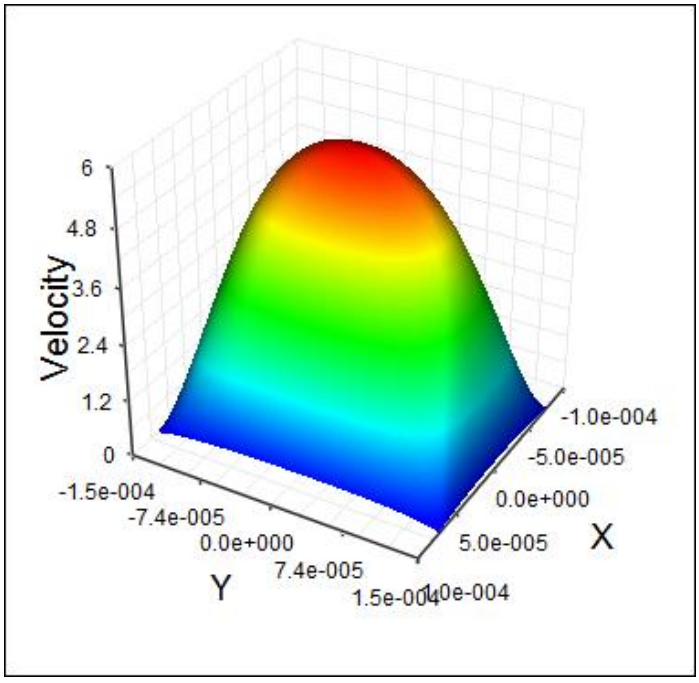

Figure 17 Fully developed velocity profile for 1:2 straight microchannel

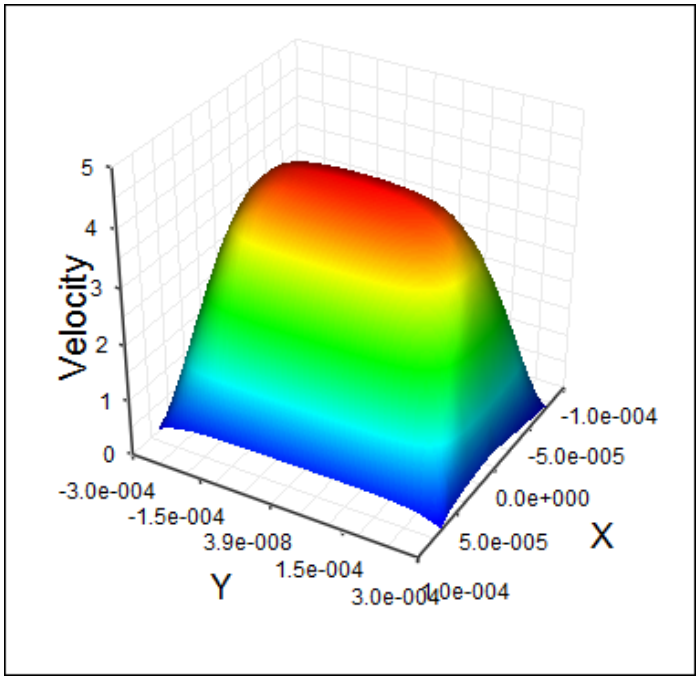

Figure 18 Fully developed velocity profile for 1:4 straight microchannel

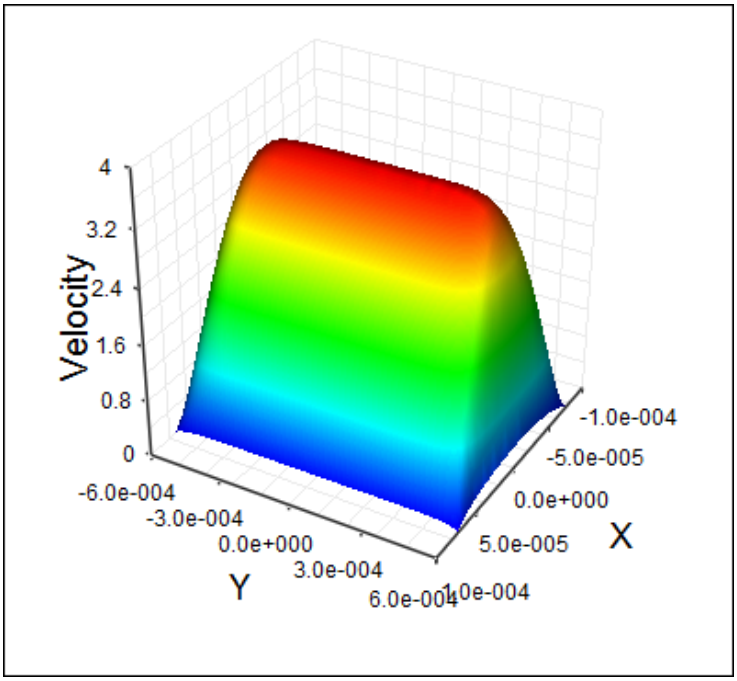

Figure 19 Fully developed velocity profile for 1:8 straight microchannel

4.3.1 Results using H1 boundary condition

First, single phase fluid flow was simulated in microchannels considering just three aspect ratios. Nusselt number as a function of axial distance in shown in Figure 20 for the three geometries considered.

It can be seen from Figure 20 that the Nusselt number is highest for 1:8 microchannel and it takes almost about the same dimensional distance to become fully developed. Once the single phase fluid was simulated, PCM fluid was also considered by changing the specific heat within the melting range (309-310 K). Also, the heat flux applied at the wall was adjusted so that the phase change process could start only after the flow was thermally fully developed. This enabled to separate the phase change effects from the entry length effects. The Nusselt number results using single phase fluid (SPF) and PCM fluid for 1:2 microchannel was compared as shown in Figure 21.

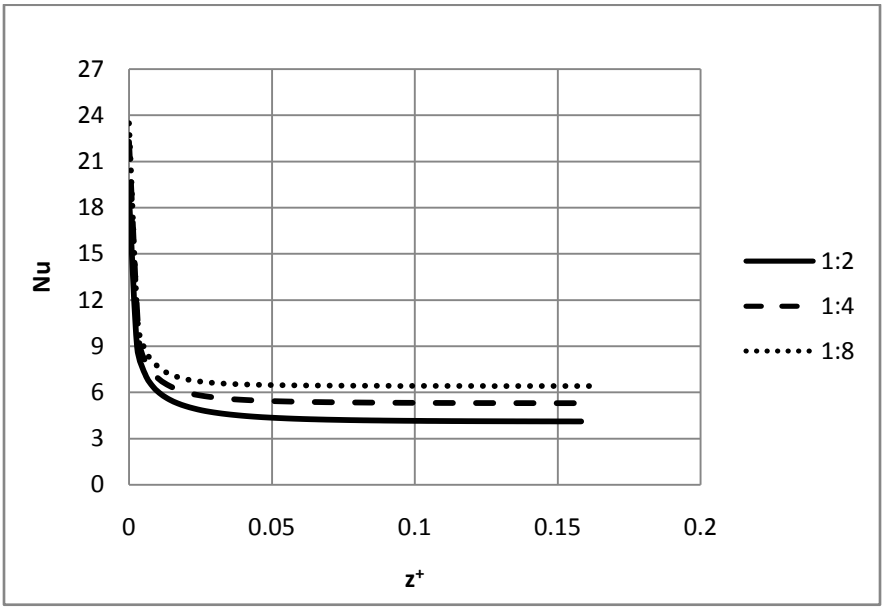

Figure 20 Nusselt number under H1 boundary condition using SPF

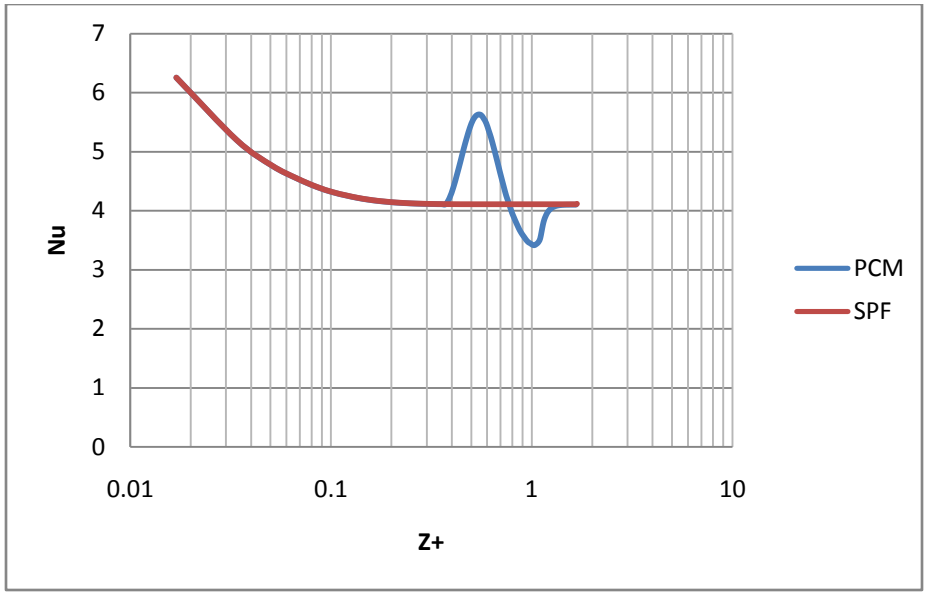

Figure 21 Nusselt number for 1:2 microchannel under H1 boundary condition

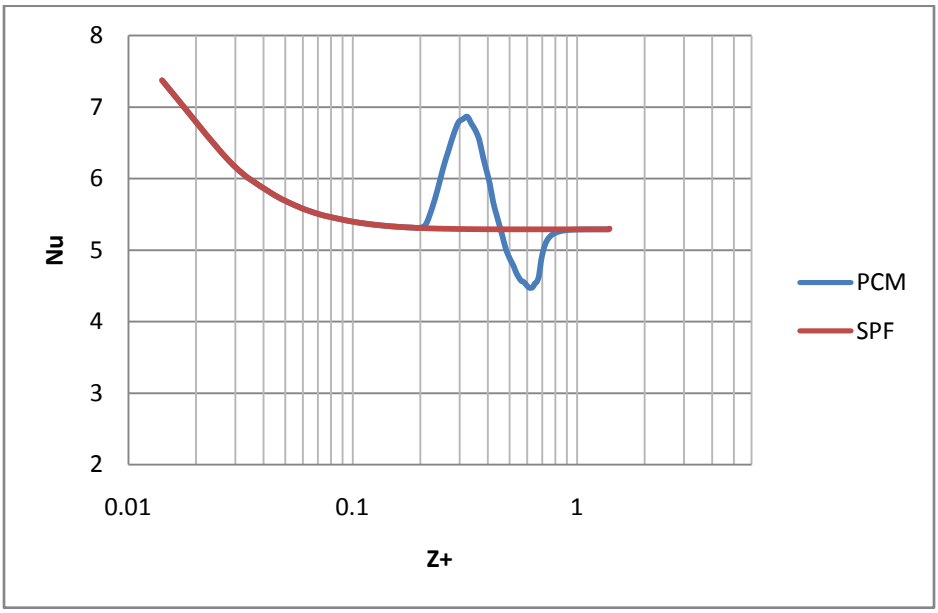

Figure 22 Nusselt number for 1:4 microchannel under H1 boundary condition

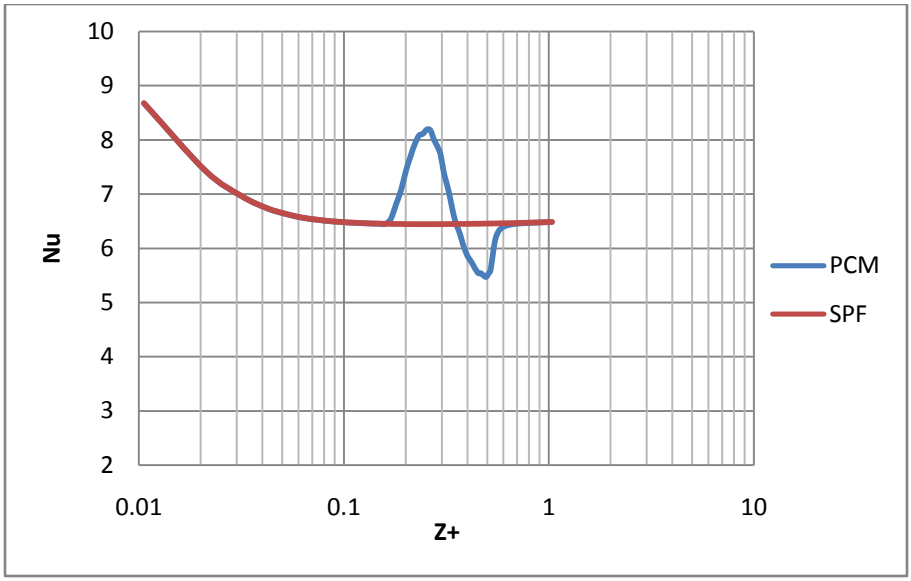

Figure 23 Nusselt number for 1:8 microchannel under H1 boundary condition

Figure 22 and Figure 23 show the Nusselt number variation with non-dimensional distance for 1:4 and 1:8 microchannels respectively under H1 boundary condition. It can be seen that in all the channels, the Nusselt number first increases and then decreases. The increase and then a decrease in the Nusselt number was also observed by Ravi [23] and can be explained as follows. The phase change process starts when the fluid temperature reaches 309 K. Since the wall temperature is higher, fluid temperatures will be higher near the wall and lower near the center of the microchannel. Hence, phase change process starts first near the walls and then propagates towards the center. In the similar fashion, phase change process ends first near the walls, and later on ends near the center of the channel. This process is depicted in Figure 24.

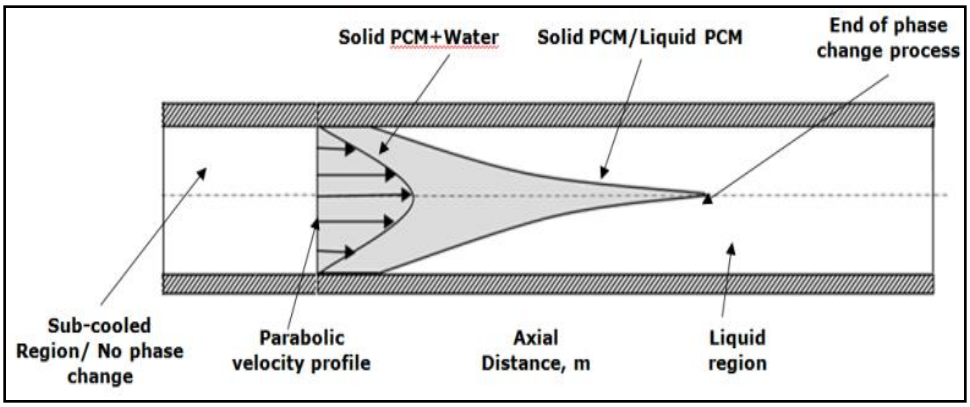

Figure 24 Phase change process in a circular channel [23]

Since the phase change starts first near the wall, during the initial region, wall temperature slowly increases while the fluid bulk temperature increases. This decreases the difference (T_w-T_b), results in higher heat transfer coefficient (since the heat flux remains constant) and higher Nusselt number. In the similar fashion, at the end of the phase change process, all the melting has already taken place near the center of the channel. This results in almost constant (or slowly increasing) bulk temperature and hence the difference between the wall and bulk temperature (T_w-T_b) increases. As the temperature difference increases, heat transfer coefficient decreases, resulting in a lower than normal Nusselt number, as observed in Figure 21 to Figure 23. Though the Nusselt number first increases and then decreases, it can be observed that the overall Nusselt number is higher, showing that PCM enhances heat transfer.

4.3.2 Results using H2 boundary condition

The same process is repeated using the H2 boundary condition. Heat flux was adjusted so that the melting process could start only after the flow was thermally fully

developed. Nusselt number was compared for SPF and PCM fluid for 1:2 and 1:4 microchannels in Figure 25 and Figure 26 respectively. It can be observed that the Nusselt number behaves in the same fashion for H1 and H2 boundary conditions, first increasing and then decreasing before reaching a constant value at the end of the phase change process. However, the difference between the maximum Nusselt number and the normal Nusselt number is highest for 1:8 microchannel as can be observed in Figure 27.

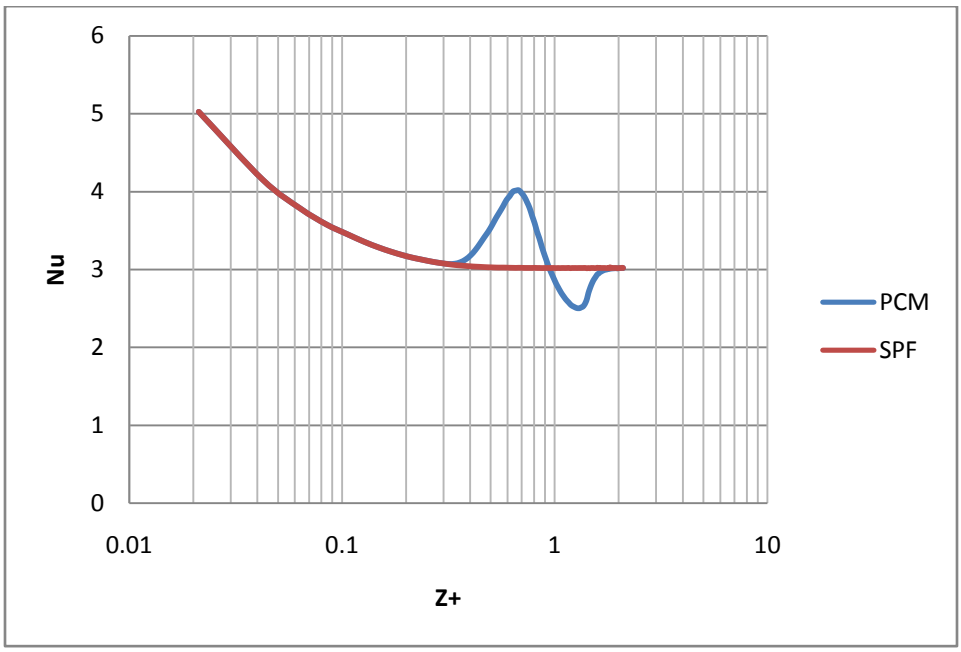

Figure 25 Nusselt number for 1:2 microchannel under H2 boundary condition

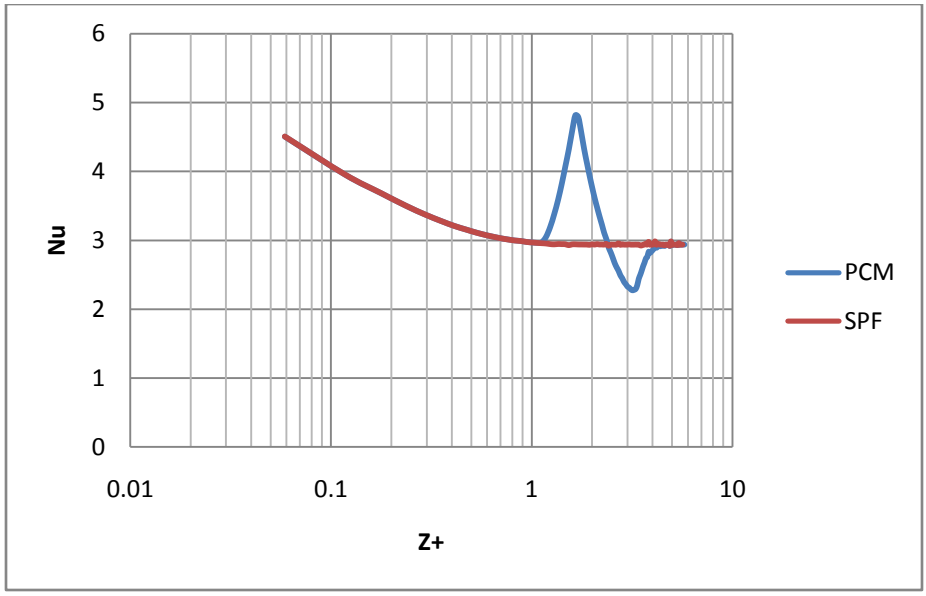

Figure 26 Nusselt number for 1:4 microchannel under H2 boundary condition

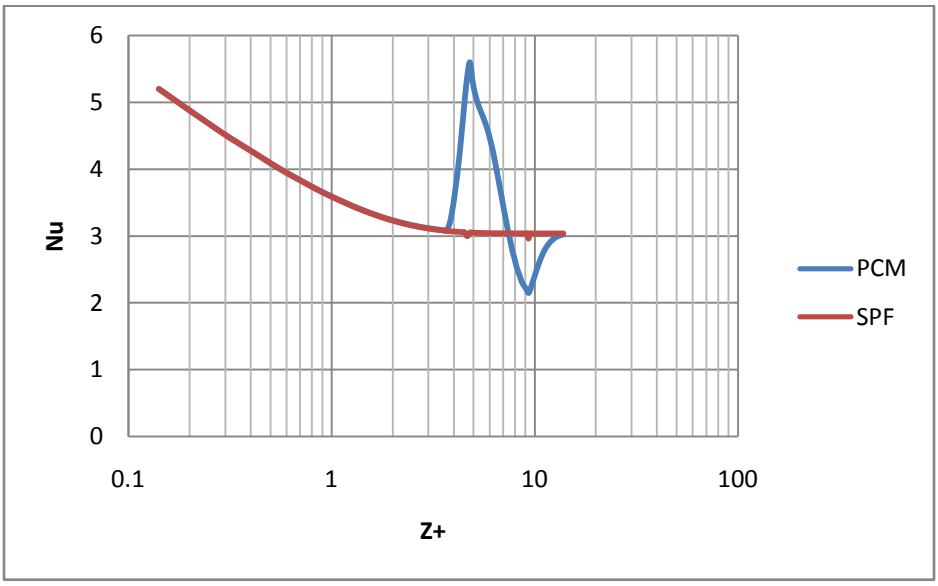

Figure 27 Nusselt number for 1:8 microchannel under H2 boundary condition

In the case of H2 boundary condition, temperature along the radial periphery of the wall (at a fixed axial distance) is not constant. Figure 28 shows how wall temperature

varies along the radial periphery for the 1:4 microchannel. Position 1 shows temperature at the center of the longer edge, while position 2 shows temperature at the corner of the wall, and position 3 shows temperature at the center of the shorter edge. It should be noted that due to symmetry only a quarter of the wall temperature is being shown. For the rest of the wall, the pattern simply repeats itself.

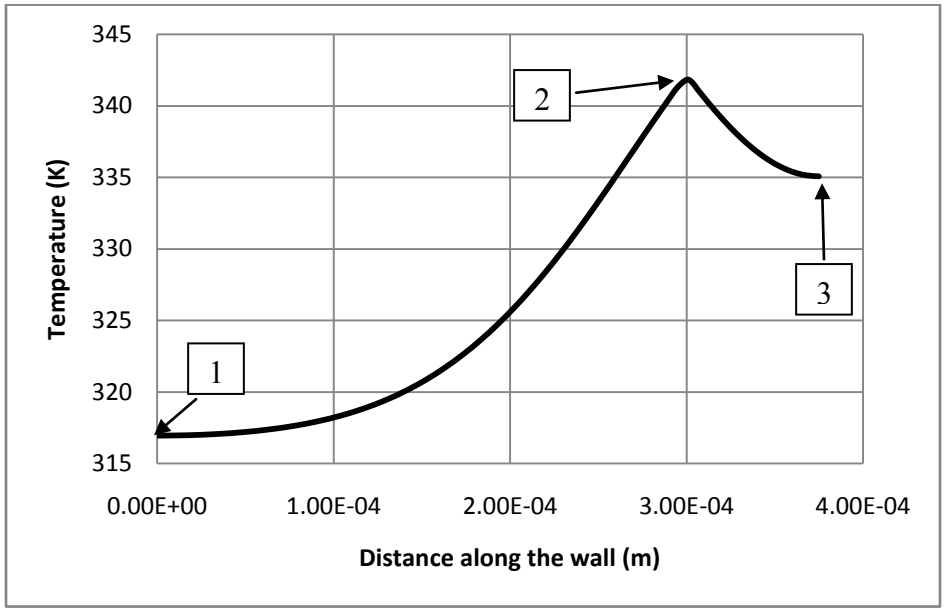

Figure 28 Temperature variation along the periphery for 1:4 microchannel

4.3.3 Results using T boundary condition

For the constant wall temperature (T) boundary condition, a specified temperature was applied at all the wall surfaces. Unlike the case of H1 and H2 boundary condition, it is difficult to separate the thermal boundary layer development and phase change process when using T boundary condition. This is because, for the T boundary condition, the flow is thermally fully developed when the fluid reaches the wall

temperature, and once the flow reaches that temperature, there will not be any (or very low) heat flux, and the phase change process takes much longer to complete.

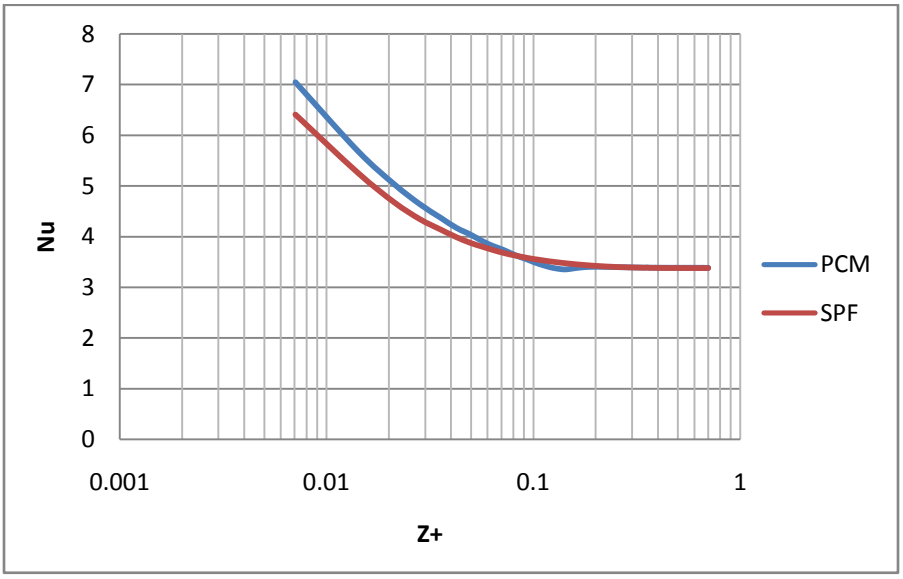

Figure 29 Nusselt number for 1:2 microchannel under T boundary condition

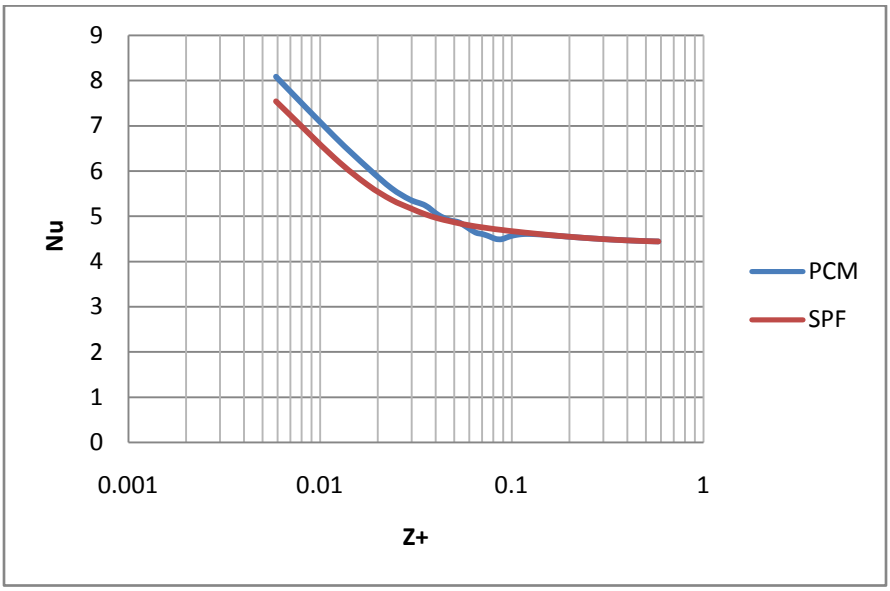

Figure 30 Nusselt number for 1:4 microchannel under T boundary condition

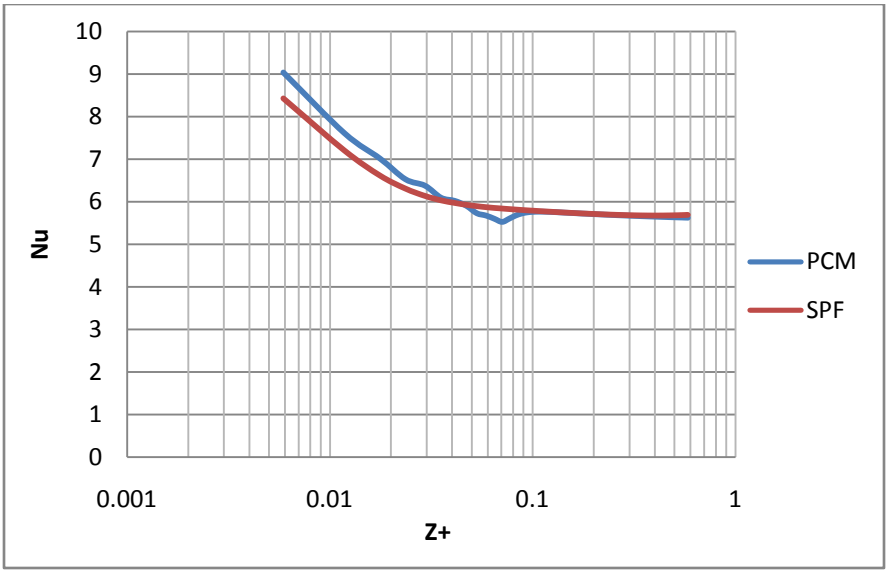

Figure 31 Nusselt number for 1:8 microchannel under T boundary condition

Figure 29 to Figure 31 show the Nusselt number variation for 1:2, 1:4 and 1:8 aspect ratio microchannels. It can be observed that the Nusselt number when using PCM fluid is higher than using SPF fluid. Furthermore, when the phase change process is near completion, it results in a radial temperature distribution dominated by the melting point of the phase change material which results in a decrease in Nusselt number.

4.4 Results using staggered pin microchannels

In the earlier section, results for the straight microchannels with three different aspect ratios were presented. This section presents results using the microchannels with staggered pins with square and circular cross sections. Conjugate heat transfer was considered and the solid domain was modeled as shown in Figure 7 and Figure 9.

Three different Reynolds numbers were considered. Since two ways of calculating the hydraulic diameter were used as explain in section 3.2.2, the corresponding Reynolds numbers and the resulting Nusselt numbers for these ways of calculation are given in Table 8. It can be observed that the Reynolds number and Nusselt number vary by a factor of 3 for the two calculation methods. This is because; the inlet hydraulic diameter is three times the pin hydraulic diameter for both circular and square pin microchannels. For the no-pins case, there is no such difference as only the inlet hydraulic diameter exists.

Table 8 Difference between parameters based on inlet and pin hydraulic diameters

Reynolds Number		Circular Pins		Square Pins		No Pins
Re_i	Re_p	Nu_i	Nu_p	Nu_i	Nu_p	Nu_i
150	50	22	7.5	12	4	3.6
200	66.7	30	10	12	4	3.6
250	83.3	40	13	12	4	3.6

Along with three different Reynolds numbers, two wall boundary conditions were considered including 1) constant heat flux (CHF) and 2) constant wall temperature (CWT). It should be noted that, as explained in section 3.1.4, H1 and H2 boundary conditions are different from the constant heat flux boundary condition used for pin-fin heat exchangers. In pin-fin heat exchangers, CHF was only applied on the base of the microchannel. For straight microchannels, the constant temperature was applied at the

wall with zero-thickness, while for staggered pin microchannels, conjugate heat transfer was considered by applying constant temperature at the bottom surface and away from the fluid-solid interface.

4.4.1 Pressure drop when using staggered pins

While pins are used to enhance heat transfer, they increase pressure drop as they act like flow obstructions. To know the effect of having pins on pressure drop, it is necessary to compare pressure drop in the presence and absence of pins. Table 9 shows pressure drop for square pins, circular pins and no-pin microchannels.

Table 9 Pressure drop for staggered pin microchannels

	Square Pins (kPa)	Circular Pins (kPa)	No Pins (kPa)
$Re_p = 50$	37.0	28.6	6.1
$Re_p = 66.7$	49.9	40.4	8.1
$Re_p = 83.3$	62.9	53.2	10.2

It can be observed from Table 9 that the pressure drop increases with Reynolds number for any geometry. Also, pressure drop is highest when using square pins, followed by circular pins and no-pins geometry.

4.4.2 Effect of fluid – PCM versus SPF

This section presents results for square and circular pinned microchannels for a Reynolds number of 66.7. First, results using the CHF boundary condition are presented followed by results using the CWT boundary condition. Figure 32 and Figure 33 show

the pin-diameter based Nusselt number for square and circular pins microchannels. It can be observed that PCM enhances heat transfer significantly for the two microchannels.

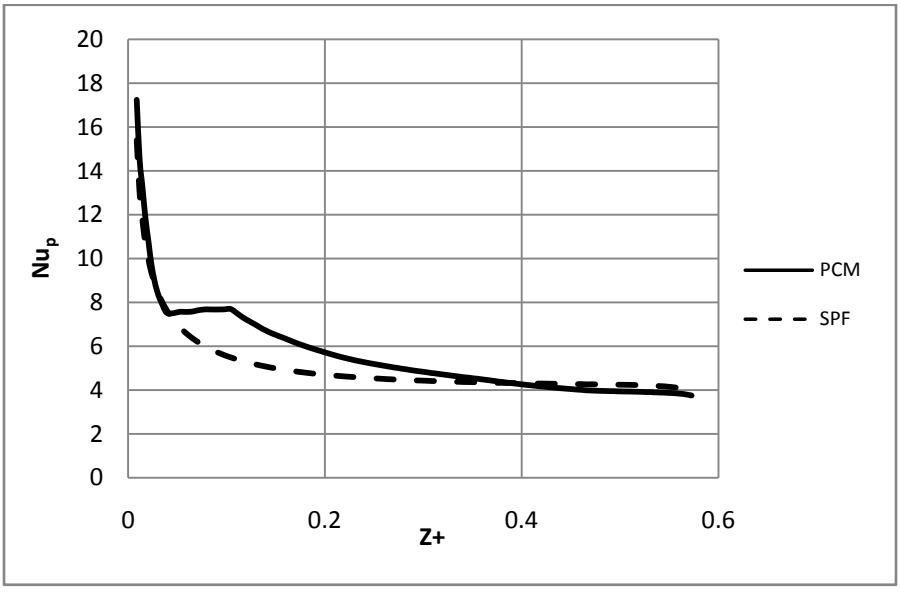

Figure 32 Nusselt number for square pins geometry using CHF boundary condition

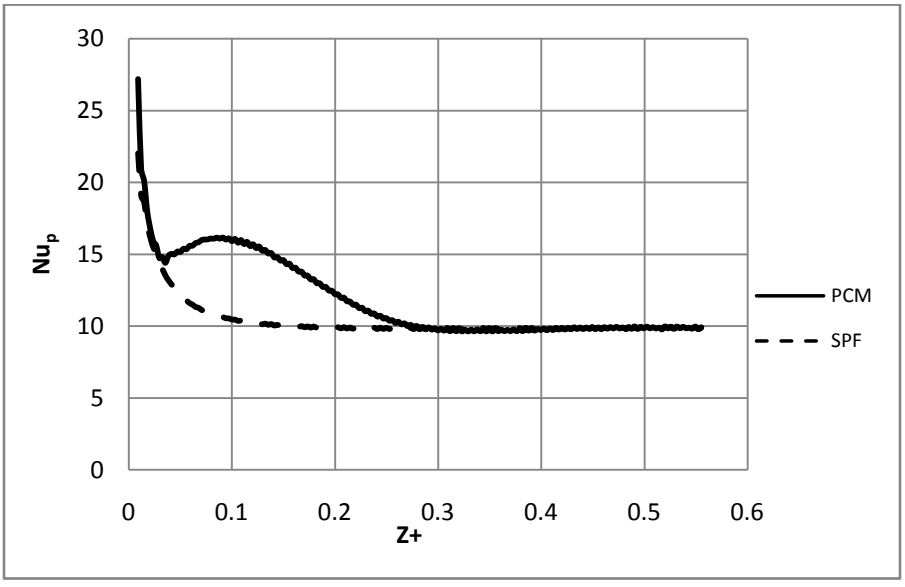

Figure 33 Nusselt number for circular pins geometry using CHF boundary condition

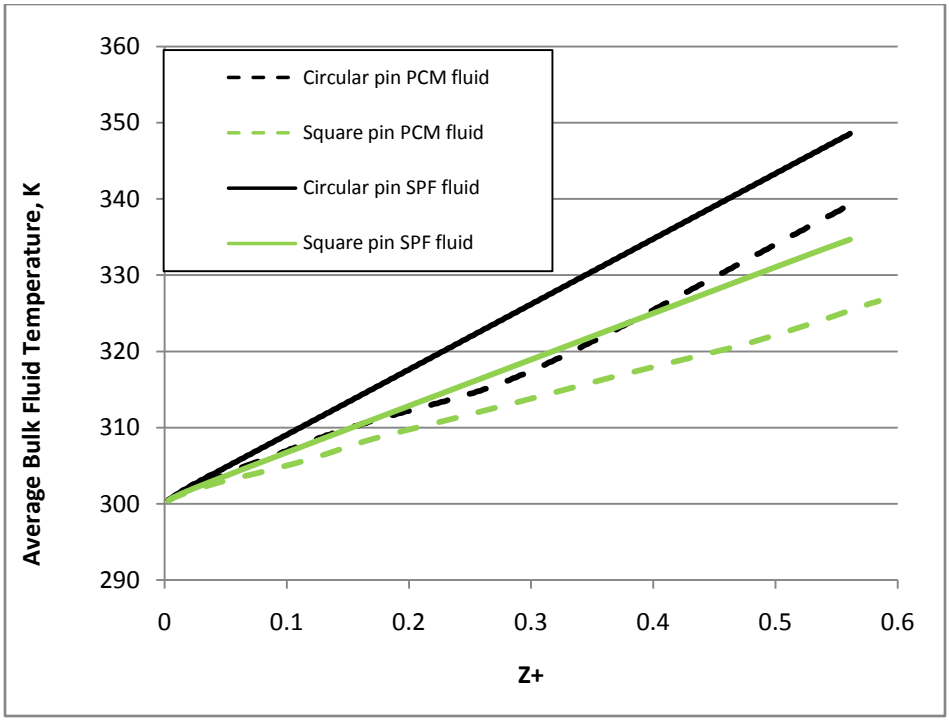

Figure 34 Fluid temperature variation for CHF boundary condition

It can be observed from Figure 32 and Figure 33 that the phase change process enhances the Nusselt number by holding back the fluid temperature as depicted in Figure 34. Also, the heat transfer enhancement is more pronounced in the case of circular case compared to the square pins because, the wake region (where the fluid is stagnant) is smaller in the case of circular pins compared to square pins as shown in Figure 35 and Figure 36. Figure 37 and Figure 38 show the velocity vectors for both square and circular pins cases. It can be observed from the color of the velocity vectors that the velocity behind the pins is very small. Also by observing Figure 38, it can be said that majority of the flow goes straight through the microchannel and parallel to the lateral faces of the pins with a small fraction of flow undergoing recirculation between the pins.

However, a different flow structure with greater vortex shedding should be expected if the pins are arranged in a way where the large vectors encounter orthogonal pin faces instead of parallel pin faces. Such a pin arrangement would probably result in greater heat transfer at the expense of significantly higher pressure drop penalty. Different pin arrangements should be considered in future studies.

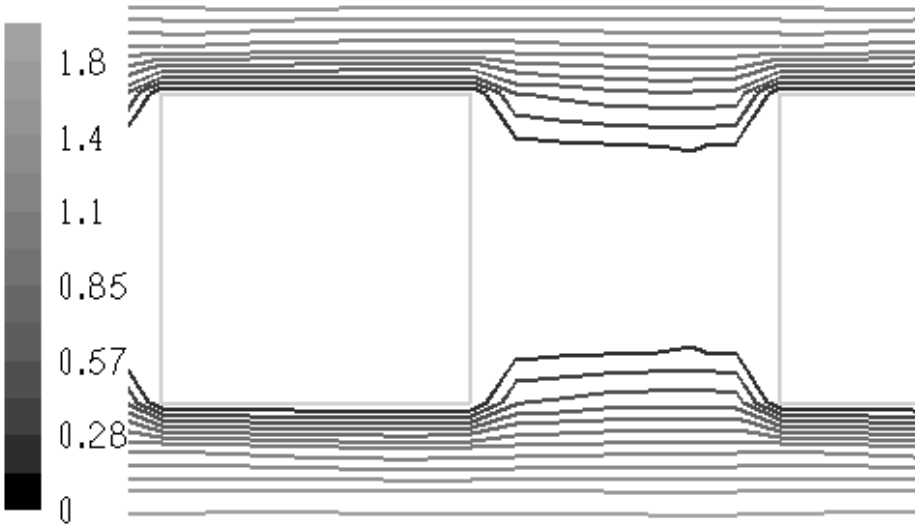

Figure 35 Contours of velocity around the square pins

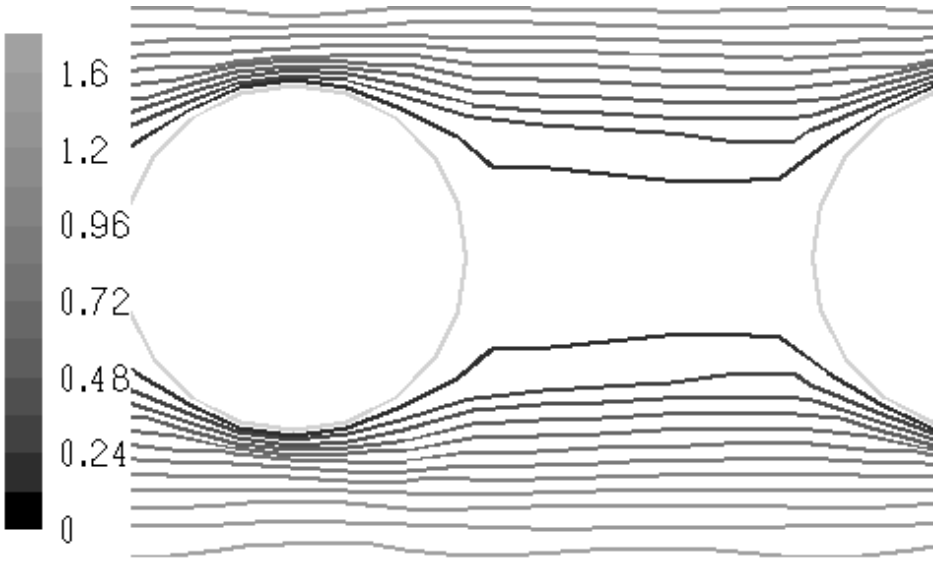

Figure 36 Contours of velocity around circular pins

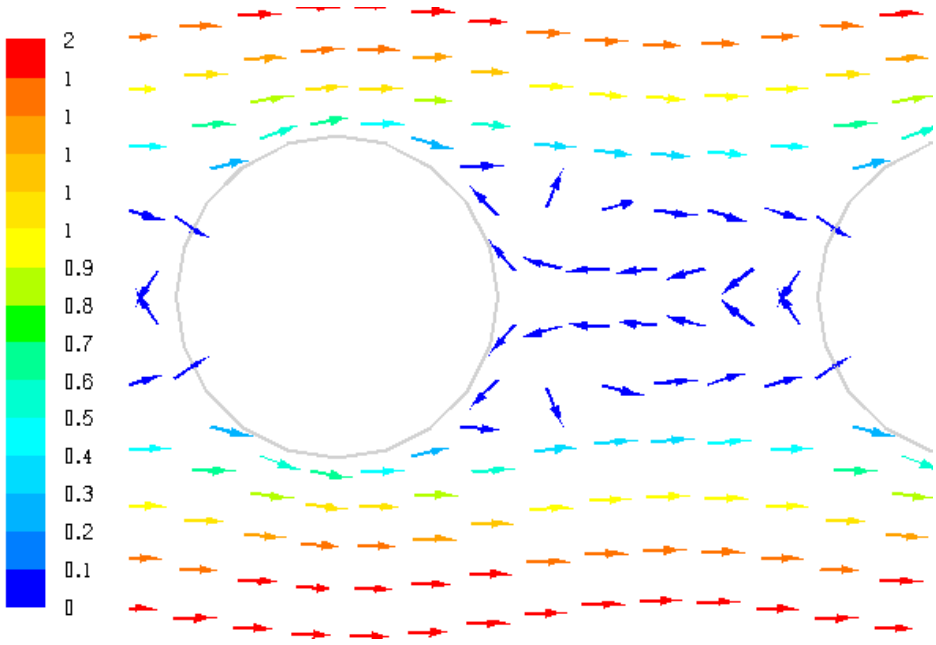

Figure 37 Velocity vectors for circular pins case at a Re_p of 50

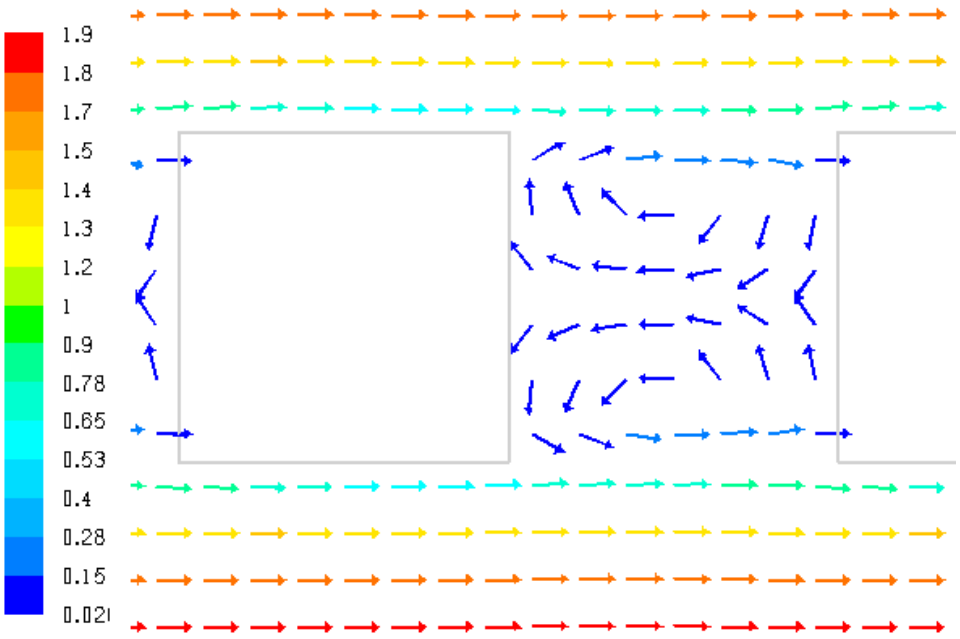

Figure 38 Velocity vectors for square pins case at Re_p of 50

Figure 39 and Figure 40 show pin-based Nusselt number for square and circular pin microchannels under CWT boundary condition. The effect of PCM on Nusselt number is higher in the case of CHF boundary condition compared to the CWT boundary condition. In the case of CHF boundary condition, the wall temperature increases, while in the case of CWT boundary condition, the wall temperature remains constant. Hence, the driving potential for the phase change process becomes stronger with the distance in the CHF case compared to the CWT case. This is consistent with the observation made by Kondle et al. [24] in the case of straight microchannels.

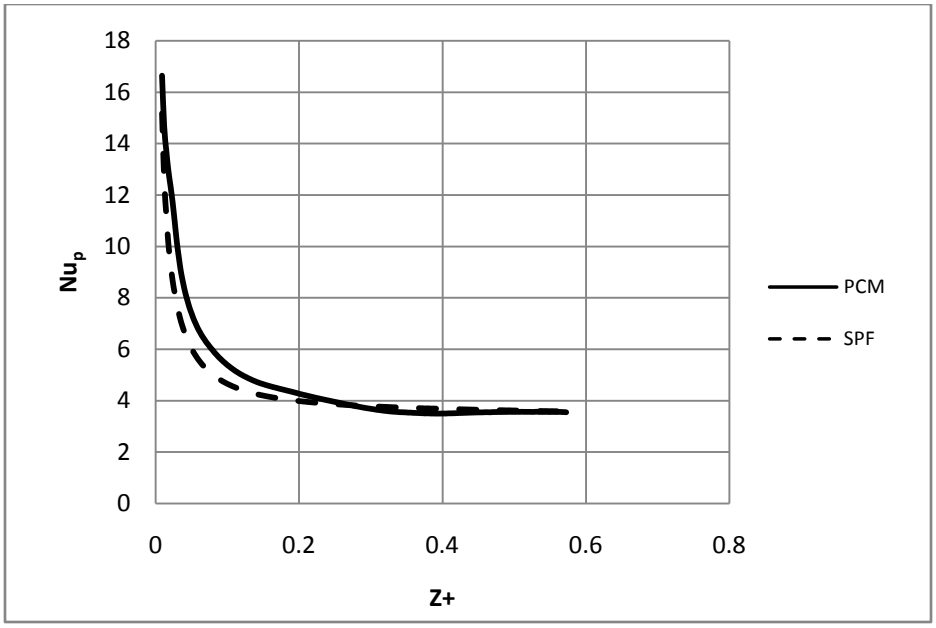

Figure 39 Nusselt number for square pins case under CWT boundary condition

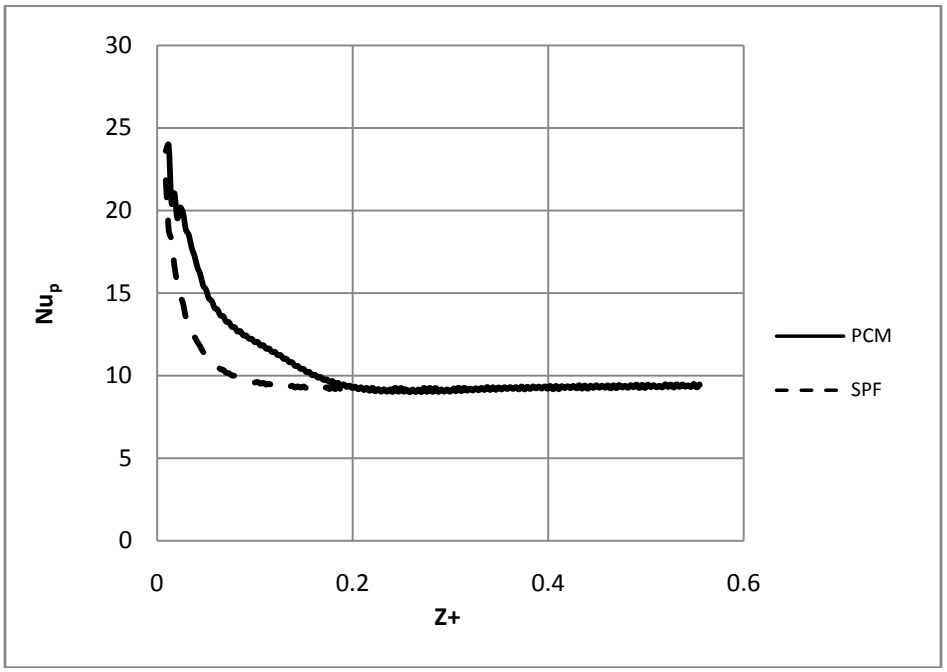

Figure 40 Nusselt number for circular pins case under CWT boundary condition

4.4.3 Comparison between different microchannel geometries

This section presents comparison between square pin, circular pin and no-pins microchannels under identical boundary conditions. Comparing these three geometries shows the effect of having pins on the overall heat transfer process. From Table 9, it was observed that the pressure drop is highest when using square pins and lowest when no pins are used. In a similar fashion, this section compares the heat transfer characteristics by comparing the Nusselt number. The results presented are for a pin-based Reynolds number of 66.7.

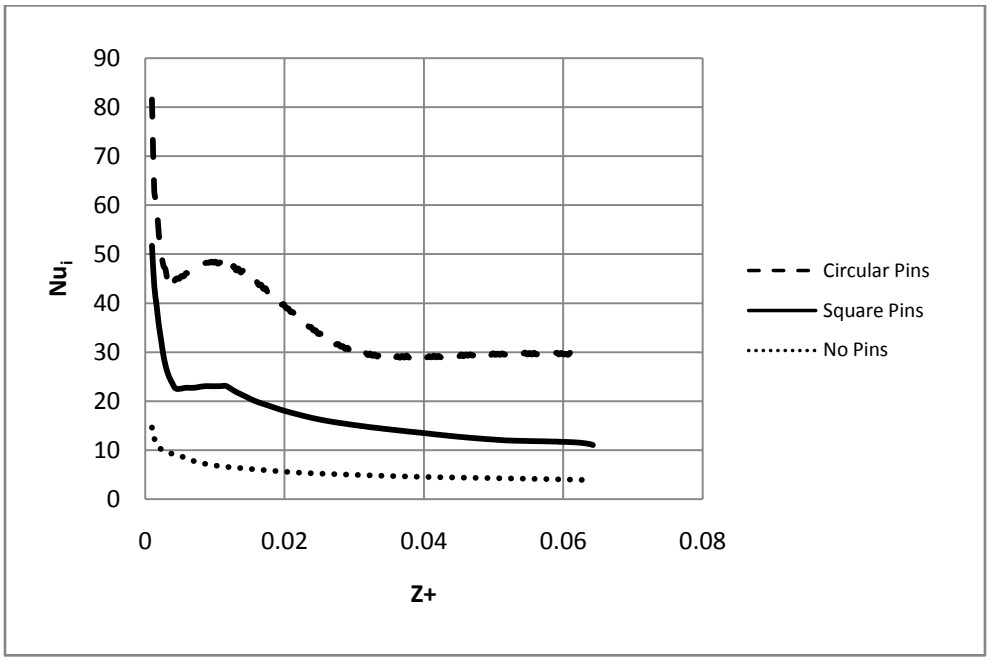

Figure 41 Nusselt number using PCM fluid under CHF boundary condition

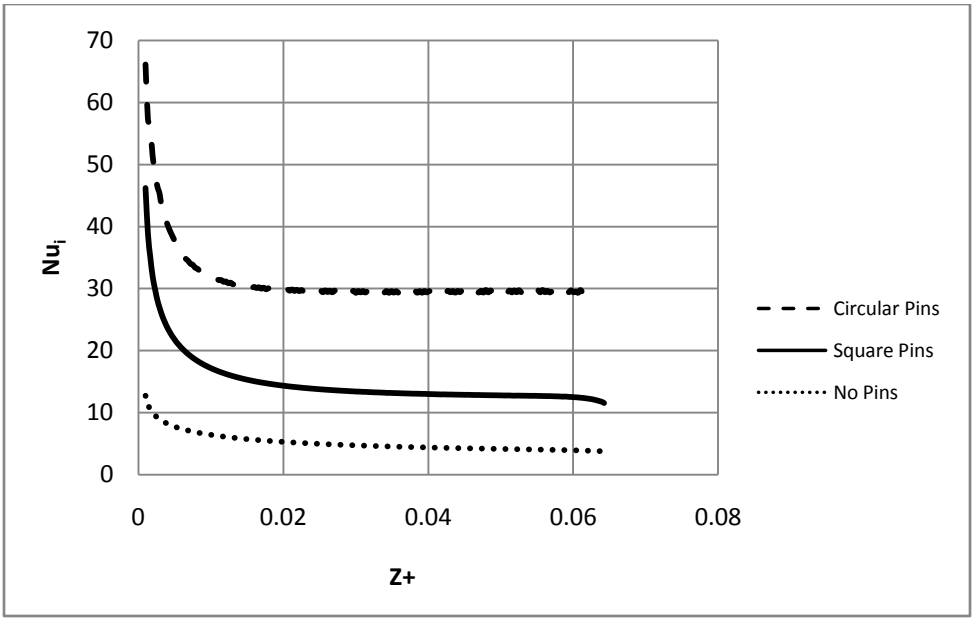

Figure 42 Nusselt number using SPF under CHF boundary condition

Figure 41 compares the Nusselt number based on inlet hydraulic diameter (Equation 10) for different geometries using PCM fluid under CHF boundary condition. Here, Nu_i is used instead of pin-based Nusselt number (Nu_p), so that the results from the no-pins case can be compared with results from circular and square pin cases. Figure 42 compares the Nusselt number using SPF fluid under the CHF boundary condition. The circular pins case exhibits higher Nusselt number compared to the square pins case. Similar behavior was observed by Soodphadke et al. [25] in the case of single phase fluids. The enhancement in Nusselt number is due to the difference in the flow structure for the square and circular pin cases. The wake region (where the fluid is stagnant) behind the circular pins is smaller than the wake region behind the square pins, as can be observed from Figure 35 and Figure 36.

4.4.4 Effect of Reynolds number

This section presents comparison between Nusselt numbers for three different Reynolds numbers. The pin-based Reynolds numbers considered were 50, 66.7 and 83.3. Figure 43 and Figure 44 show Nusselt number variation for three different Reynolds numbers under CHF boundary condition using SPF fluid and two microchannel geometries.

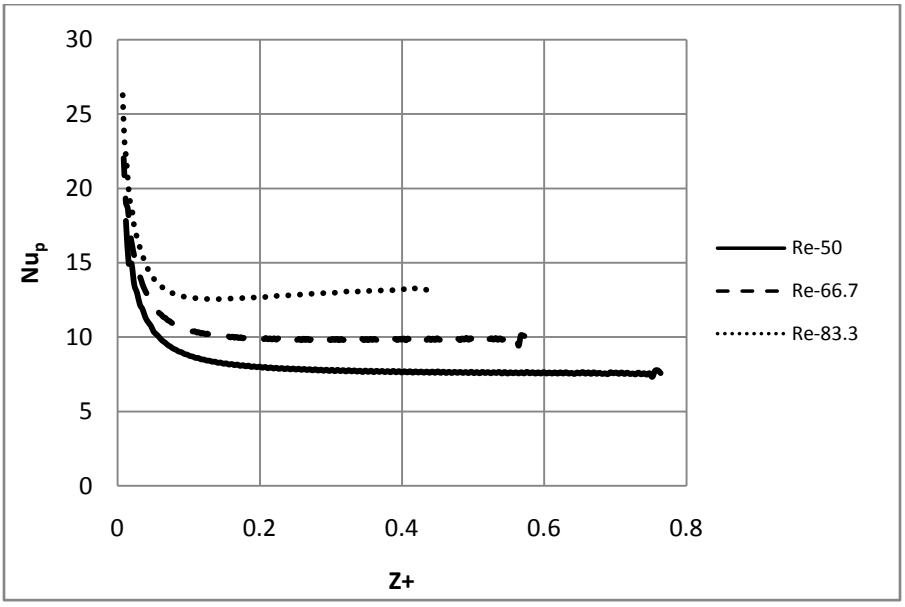

Figure 43 Nusselt number for circular pins geometry for SPF

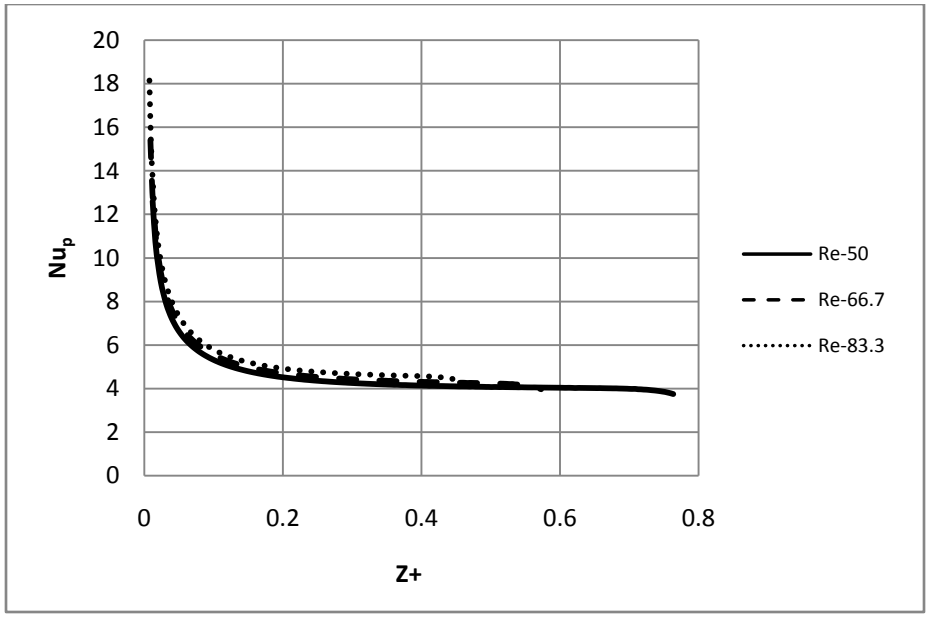

Figure 44 Nusselt number for square pins geometry for SPF

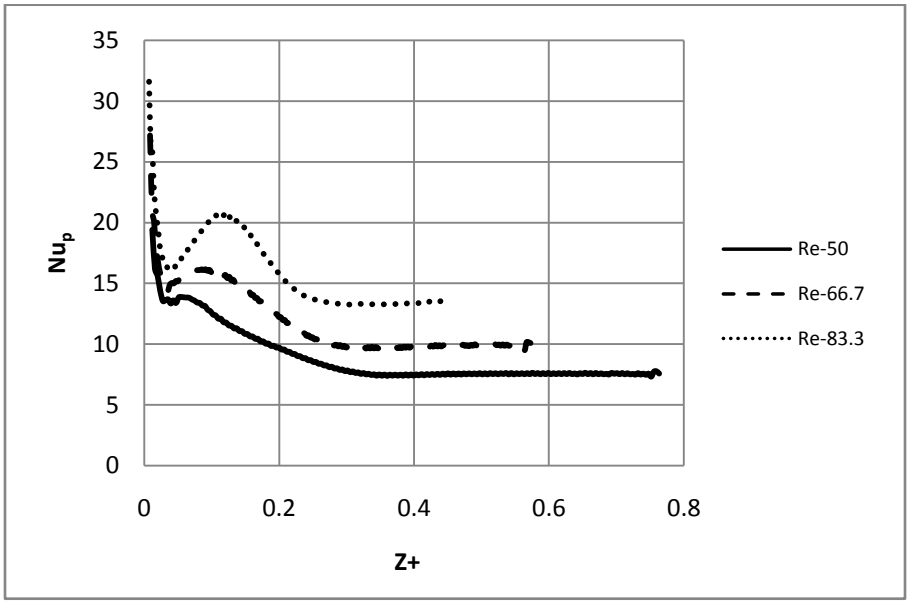

Figure 45 Nusselt number for circular pins geometry for PCM fluid

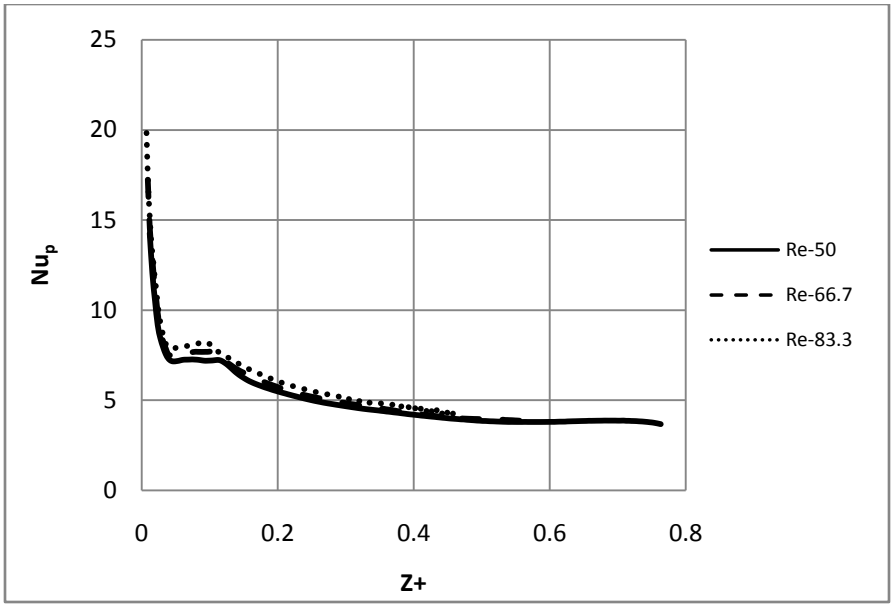

Figure 46 Nusselt number for square pins geometry for PCM fluid

Figure 45 and Figure 46 show Nusselt number variation for different Reynolds numbers, under CHF boundary condition using PCM fluid. It can be observed that the Nusselt number increases with Reynolds number for circular pins case, whereas it converges to the same value for all Reynolds numbers when square pins were used. For circular pins, the angle of separation is greater than in the square pin which results in greater Nusselt number. Also, periodic vortex shedding has been reported by Agaro and Comini [15] and Comini and Croce [26], which usually starts at Reynolds numbers between 55 and 80 for circular and square pins depending upon the spacing between the pins. Hence, an unsteady periodic flow analysis should be undertaken to determine if greater Nusselt number values can be achieved.

4.4.5 Effect of boundary condition

This section compares the effect of boundary condition on heat transfer. Nusselt numbers are compared between two boundary conditions, CHF and CWT for square and circular pin geometries. It can be observed from Figure 47 and Figure 48 that the Nusselt number is higher when using CHF boundary condition compared to CWT boundary condition. The reason for the higher Nusselt number in the case of CHF boundary condition compared to CWT boundary condition was explained in section 4.4.2. The results presented are for a pin-based Reynolds number of 66.7.

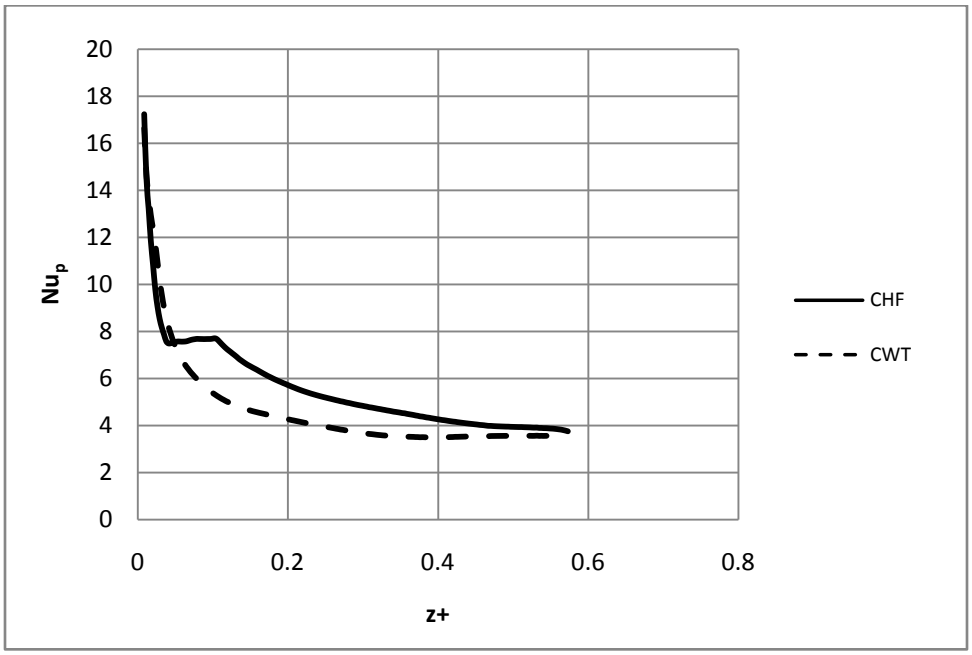

Figure 47 Nusselt number for square pins geometry under different BC(s)

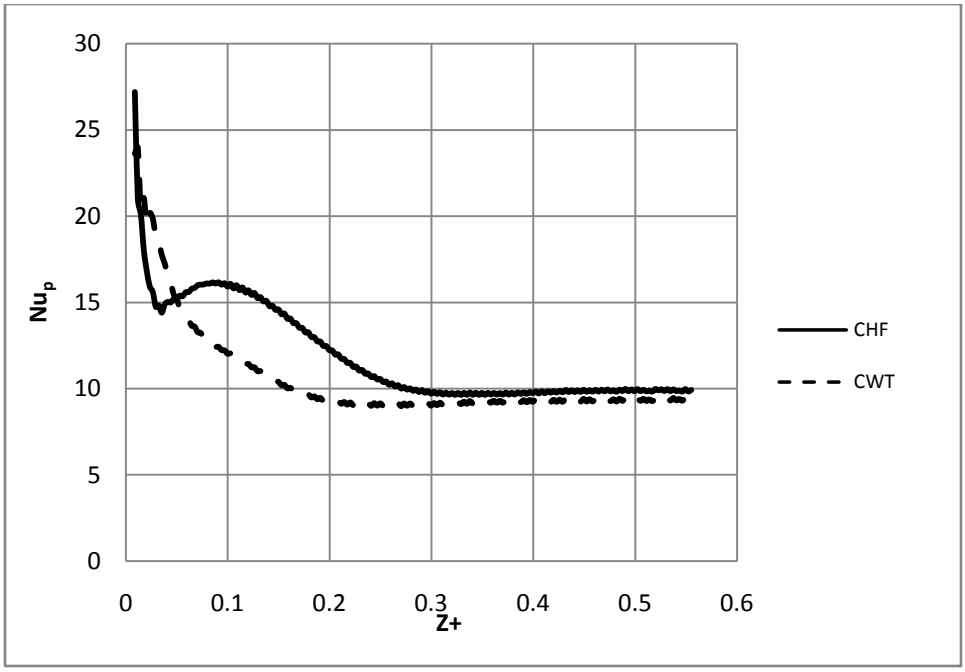

Figure 48 Nusselt number for circular pins geometry under different BC(s)

4.4.6 Thermal performance factor

The use of pins in microchannels increases the heat transfer, but also has the undesirable effect of increasing the pressure drop. It is necessary to develop and use a performance metric that considers both Nusselt number and friction factor (pressure drop) in a single parameter, so that the effectiveness of having the pins in the geometry can be compared. Such a parameter has been suggested by Saha and Acharya [27] and Agaro and Comini [15] is given by,

$$\eta = \frac{Nu/Nu_{ch}}{\left(f/f_{ch}\right)^{1/3}} \tag{22}$$

where,

Nu_{ch} = Characteristic Nusselt number, which in this case is equal to the no-pins case Nusselt number

f_{ch} = Characteristic friction factor, which in this case is equal to the no-pins case friction factor

This performance factor has been compared for the square and circular pin cases for several Reynolds numbers as shown in Table 10. It can be observed from the table, that the performance factor is highest for the circular pins. For the circular pins case, the performance factor increases with Reynolds number, whereas it remains almost constant for square pins case. In the circular-pin case, the angle of separation is greater which results in greater Nusselt number and lower pressure drop (lesser drag). Also, the performance factor is higher for both the pin fin cases compared to the no-pins case.

Table 10 Thermal performance factors for the three geometries

	Square Pins	Circular Pins
$Re_i = 150$	1.83	3.65
$Re_i = 200$	1.82	4.90
$Re_i = 250$	1.82	6.41

5. CONCLUSION

The following conclusions can be made from the results and discussion from this study:

- Higher pressure drop is observed in the case of square pins compared to circular pins

- The fully developed flow Nusselt number is higher for H1 boundary condition than for H2 or T boundary conditions for all aspect ratios considered for the straight microchannels in the study.

- The Nusselt number was found to increase when using PCM fluid compared to a single phase fluid (water) for all the geometries considered.

- The specific heat model predicts the heat transfer behavior accurately when compared with experimental results.

- The trend in Nusselt number during the phase change process was found to be same for both H1 and H2 boundary conditions for the straight microchannels.

- For H1 and H2 boundary conditions, Nusselt number was found to increase during the beginning of phase change process and dropped (lower than for the SPF) considerably as the phase change process was near completion for the straight microchannels.

- The axial distance required to obtain fully developed flow is much higher for H2 boundary condition compared to H1 boundary condition when taking into account the phase change process of the PCM fluid for the straight microchannels.

- When using PCM fluid, the difference between the peak value and fully developed values of Nusselt number is higher for H2 boundary condition than for H1 boundary condition.

- Nusselt number is higher for circular pins compared to square pins in the Reynolds number range considered.

- The effect of the phase change process on heat transfer is found to be higher in the case of circular pins compared to square pins. This can be observed by the increase in the Nusselt number with PCM fluid compared to SPF fluid for the same geometry.

- The effect of phase change process on Nusselt number is found to be higher under CHF boundary condition compared to CWT boundary condition for both the staggered pin geometries considered.

- The axial distance required to obtain a steady Nusselt number is almost same for square and circular pins geometries.

6. FUTURE WORK

As discussed in section 4.4.4, Agaro and Comini [15] have numerically investigated the unsteady periodic flow for a range of laminar Reynolds numbers. A couple of simulations with periodic flow with circular pins with a pin Reynolds number of 90 were tried in this study using Fluent. First, the same geometry (circular pins only) and the Reynolds number that Agaro and Comini [15] used were taken into considerations when simulating periodic flow in Fluent. However, the exact boundary conditions could not be imposed since Fluent is not capable of specifying and imposing periodic flow in more than one axial direction. In their study, they applied periodic conditions in two directions, one along the main flow direction and other perpendicular to the flow. Fluent does not allow periodic boundaries in two directions. To overcome this limitation, more number of pins was considered in both the directions.

The geometry that they used consisted of a unit cell with one whole pin and two half pins. When using Fluent, the geometry modeled was such that it contained 5 unit cells in the transverse direction, and 7 unit cells in the flow direction. The pin dimensions, spacing between the pins and material properties were same as the one specified in the publication by Agaro and Comini [15]. Though a total number of 35 (5x7) cells were considered, the results were taken only from the center (3x4) cell to minimize wall boundary effects. Two boundary conditions including non-slip and symmetry were applied at the lateral boundaries. Since, only the solution from the center

cell was extracted, the two approaches (i.e. Agaro and Comini and this study) led to almost the same average Nusselt number.

Thermal boundary condition of constant wall temperature (340 K) was specified at the wall. Mass flow rate was specified using the periodic condition option in Fluent. The Nusselt number was calculated using the approach outlined by Agaro and Comini [15]. The Nusselt number variation with non-dimensional time is shown in Figure 49 using the same spacing between the pins reported by Agaro and Comini [15]. Once the same geometry was simulated, the spacing was increased by 20% (in the transverse direction) resulting in a lower Nusselt number as shown in Figure 50.

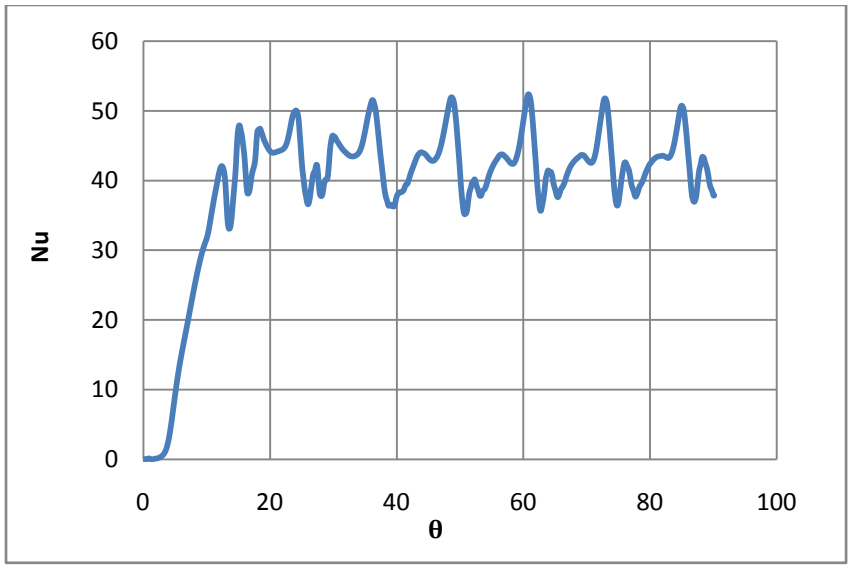

Figure 49 Nusselt number for unsteady periodic flow with Reynolds number of 90

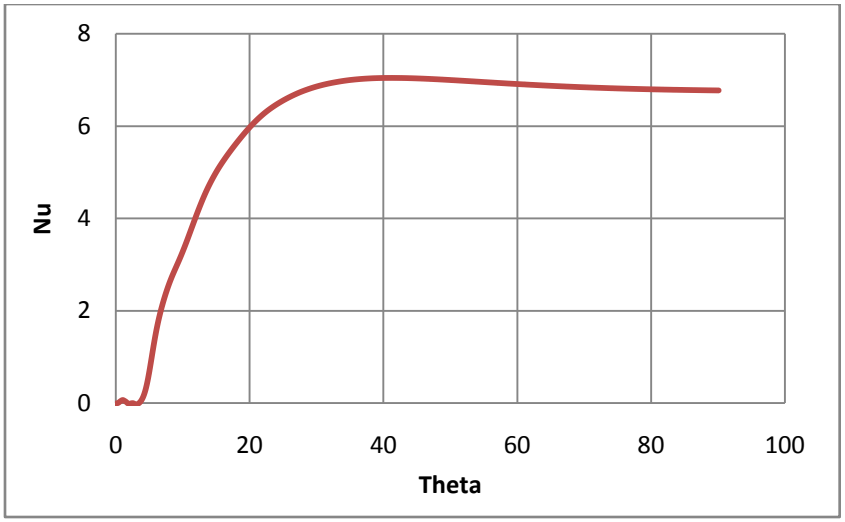

Figure 50 Nusselt number after the increase in spacing by 20% with Re of 90

The average Nusselt number for the first spacing (Figure 49) is about 42.6, which is very close to the average value of 43 reported by Agaro and Comini [15]. The periodic variation in Nusselt number is due to the presence of periodic vortex shedding, as shown in Figure 51. Though the average value is same, the frequency and amplitude of the Nusselt number (or vortex shedding) are found to be different from the reported values [15]. This is due to the limitation in Fluent that does not allow periodic flow in more than one direction.

From Figure 49 and Figure 50, it can be observed that the Nusselt number varies in a periodic fashion for the first spacing (141 μm), while it reaches a constant value when the spacing is increased by 20% (Figure 50). This shows that the change in spacing affects the flow structure which becomes steady as shown in Figure 52 without any periodic vortex generation. Also, Nusselt number for steady flow from Figure 50 is about 7, which is much lower than the average value of 42.6 when the flow exhibits

periodic vortex shedding as shown in Figure 49. The difference between the average values can be attributed to the presence of vortices and the resulting constant mixing of fluid from the wall region to the core region. Fluid mixing results in higher heat transfer since the colder fluid near the center is brought near the walls. Hence, the heat transfer (Nusselt number) is higher in the presence of vortices compared to steady flow.

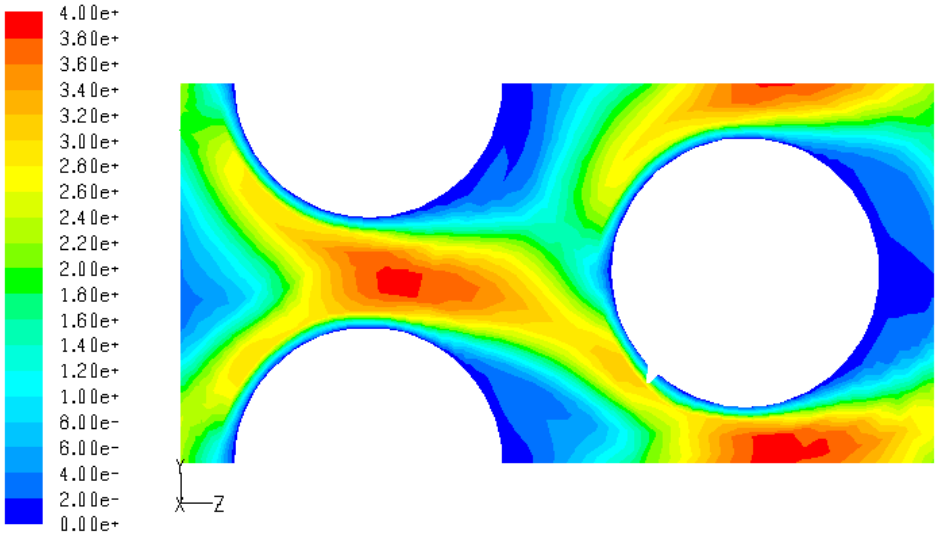

Figure 51 Velocity contour showing vortex for initial spacing with Re of 90

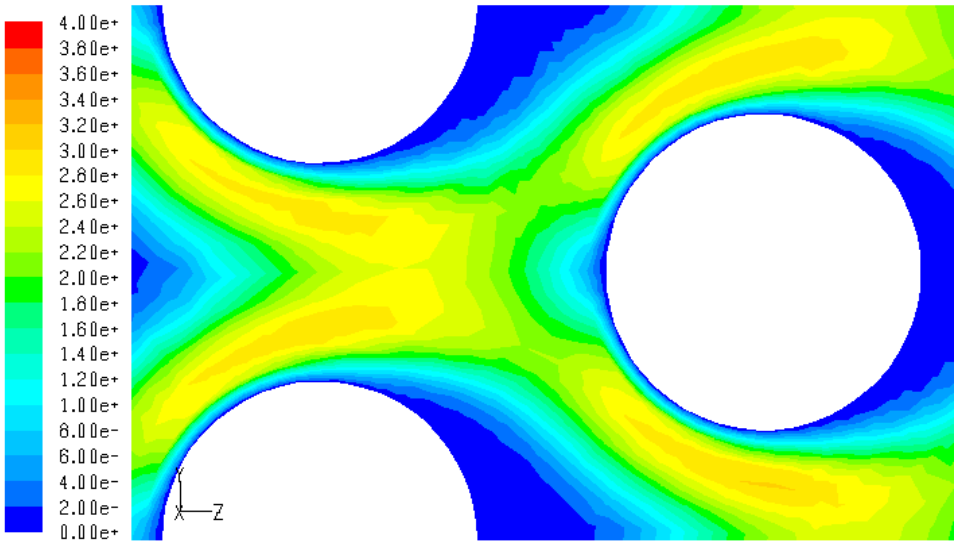

Figure 52 Velocity contour for 20% increased spacing with Re of 90

REFERENCES

1. P. S. Lee, S. V. Garimella, and D. Liu, Investigation of Heat Transfer in Rectangular Microchannels, *International Journal of Heat and Mass Transfer*, vol. 48, pp. 1608-1704, 2005.
2. X. Wei, Y. Joshi, and M. K. Patterson, Experimental and Numerical Study of a Stacked Microchannel Heat Sink for Liquid Cooling of Microelectronic Devices, *ASME Journal of Heat Transfer*, vol. 129, pp. 1432-1444, 2007.
3. P. S. Lee and S. V. Garimella, Thermally Developing Flow and Heat Transfer in Rectangular Microchannels of Different Aspect Ratios, *International Journal of Heat and Mass Transfer*, vol. 49, pp. 3060-3067, 2006.
4. Y. Yamagishi, H. Takeuchi, A. T. Pyatenko and N. Kayukawa, Characteristics of Microencapuslated PCM Slurry as a Heat-Transfer Fluid, *AIChE Journal*, vol. 45, no. 4, pp. 696-707, 1999.
5. J. L. Alvarado, C. Marsh, C. Sohn, G. Phetteplace, and T. Newell, Thermal Performance of Microencapsulated Phase Change Material Slurry in Turbulent Flow under Constant Heat Flux, *International Journal of Heat and Mass Transfer*, vol. 50, pp. 1938-1952, 2007.
6. B. Chen, X. Wang, R. Zeng, Y. Zhang, X. Wang et al., An Experimental Study of Convective Heat Transfer with Microencapsulated Phase Change Material Suspension: Laminar Flow in a Circular Tube under Constant Heat Flux, *Experimental Thermal and Fluid Science*, vol. 32, pp. 1638-1646, 2008.

7. E. L. Alisetti and S. K. Roy, Forced Convection Heat Transfer to Phase Change Material Slurries in Circular Ducts, *Journal of Thermophysics*, vol. 14, no. 1, pp. 115-118, 2000.

8. S. K. Roy and B. L. Avanic, Laminar Forced Convection Heat Transfer with Phase Change Material Suspensions, *International Communications in Heat and Mass Transfer*, vol. 28, no. 7, pp. 895-904, 2001.

9. X. Wang, J. Niu, Y. Li, X. Wang, B. Chen et. al., Flow and Heat Transfer Behaviors of Phase Change Material Slurries in a Horizontal Circular Tube, *International Journal of Heat and Mass Transfer*, vol. 50, pp. 2480-2491, 2007.

10. Y. L. Hao and Y. X. Tao, A Numerical Model for Phase-Change Suspension Flow in Microchannels, *Numerical Heat Transfer, Part A*, vol. 46, pp. 55-77, 2004.

11. R. Sabbah, M. M. Farid, and S. Al-Hallaj, Micro-channel Heat Sink with Slurry of Water with Micro-encapsulated Phase Change Material: 3D-Numerical Study, *Applied Thermal Engineering*, vol. 29, no. 2-3, pp. 445-454, 2009.

12. G. Ravi, J. L. Alvarado, C. Marsh, and D. A. Kessler, Laminar Flow Forced Convection Heat Transfer Behavior of a Phase Change Material Fluid in Finned Tubes, *Numerical Heat Transfer*, *Part A*, vol. 55, pp. 721-738, 2009.

13. R. S. Prasher, J. Dirner, J. Chang, A. Myers, D. Chau et al., Nusselt Number and Friction Factor of Staggered Arrays of Low Aspect Ratio Micropin-Fins under Cross Flow for Water as Fluid, *Journal of Heat Transfer*, vol. 129, pp. 141-153, 2007.

14. A. Kosar, C. Mishra, and Y. Peles, Laminar Flow across a Bank of Low Aspect Ratio Micro Pin Fins, *Journal of Fluids Engineering*, vol. 127, pp. 419-430, 2005.
15. P. D. Agaro and G. Comini, Thermal-Performance Evaluation of Coolant Passages with Staggered Arrays of Pin Fins, *Heat Mass Transfer*, vol. 44, no. 7, pp. 815-825, 2008.
16. Fluent 6.3 User' Guide, Fluent Inc., Lebanon, New Hampshire, 2006.
17. K. Q. Xing, Y. X. Tao, and Y. L. Hao, Performance Evaluation of Liquid Flow with PCM Particles in Microchannels, *Journal of Heat Transfer*, vol. 127, pp. 931-940, 2005.
18. P. Charunyakorn, S. Sengupta and S. K. Roy, Forced Convection Heat Transfer in Microencapsulated Phase Change Material Slurries: Flow in Circular Ducts, *International Journal of Heat and Mass Transfer*, vol. 34, no. 3, pp**.** 819–833, 1991.
19. R. K. Shah and A. L. London, Thermal Boundary Condition and Some Solutions for Laminar Duct Flow Forced Convection, *ASME Journal of Heat Transfer*, vol. 96, pp. 159-165, 1974.
20. F. P. Incropera and D. P. Dewitt, *Fundamentals of Heat and Mass Transfer*, John Wiley, New York, 2007.
21. W. M. Kays, *Convective Heat Transfer*, McGraw-Hill Inc, New York, 1966.
22. S. G. Kandlikar, S. Garimella, D. Li, S. Colin, and M. R. King, *Heat Transfer and Fluid Flow in Minichannels and Microchannels*, Elsevier, New York, 2006.

23. G. Ravi, Study of Laminar Flow Forced Convection Heat Transfer Behavior of a Phase Change Material Fluid, M.S. Thesis, Texas A&M University, College Station, Texas, 2009.

24. S. Kondle, J. L. Alvarado, C. Marsh, D. Kessler, and P. Stynoski, Laminar Flow Forced Convection Heat Transfer Behavior of a Phase Change Material Fluid in Microchannels, *Proceedings of ASME 2009 International Mechanical Engineering Congress and Exposition*, Lake Buena Vista, Florida, 2009.

25. D. Soodphakdee, M. Behnia, and D. W. Copeland, A Comparison of Fin Geometries for Heat Sinks in Laminar Forced Convection: Part-I – Round, Elliptical, and Plate Fins in Staggered and In-Line Configurations, *International Journal of Microcircuits and Electronic Packaging*, vol. 24, pp. 68-76, 2001.

26. G. Comini, and G. Croce, Numerical Simulation of Convective Heat and Mass Transfer in Banks of Tubes, *International Journal for Numerical Methods in Engineering*, vol. 57, pp. 1755-1773, 2003.

27. A. K. Saha and S. Acharya, Parametric Study of Unsteady Flow and Heat Transfer in Pin-Fin Heat Exchangers, *International Journal of Heat and Mass Transfer*, vol. 46, pp. 3815-3830, 2003.

APPENDIX A

GEOMETRY AND GRID GENERATION IN GAMBIT

1. Geometry Creation

Geometry is the actual part of the fluid and solid domain where computation is required for CFD analysis. The fluid domain represents the section where the fluid flows while the solid domain includes the solid portion, and the walls.

2. Grid Generation

Grid generation is the process of dividing the domain into small elements. Flow and heat transfer can be solved using the discretized equations in these elements. There are several different types of grids including hexahedral, tetrahedral, prisms etc., based on the shape of the elements.

Steps for creating straight microchannels:

a. Create the face directly by specifying height and width.

b. Extrude the face to the volume of required length using the face sweep.

Steps for creating staggered pin microchannels:

a. Create the half pin cross sections for square or circle.

b. Sweep the cross section to create 3-D pin of the required height.

c. Copy the pin volumes to create required number of pins.

d. Create a face such that it represents the fluid cross section when pins are not present.
e. Below this face, create another face that represents the solid domain.
f. Sweep both of these faces to the required length.
g. Split one of the newly created volumes with all other volumes (including pin volumes).

Grid (Mesh) Generation for straight microchannels:

a. Create grid on the edges of the inlet with appropriate ratios so the grid near the walls will be fine and the grid near the center of the domain is coarse.
b. Create grid on the face. Specify Quad Map for the mesh type. Since the grid on the edges is fixed, parameters specified during the face meshing are not used.
c. Create grid on the edges in the flow direction.
d. Create the volume grid using the cooper grid option.

Grid (Mesh) Generation for staggered pin microchannels:

a. Create Quad Pave mesh on the top faces of the geometry.
b. Create grid on one of the vertical edges that is connected to the fluid volume. The following three steps need to be followed in their order.
    a. Create grid for the fluid volume using the cooper tool.
    b. Create grid for the solid pins using the cooper tool.
    c. Create grid for the bottom solid domain, again using the cooper tool.

Setting Boundary and Fluid Zones in Gambit:

a. Set *Velocity Inlet* condition for the inlet face.
b. Set *Wall* condition for all the walls.
c. Set *Pressure Outlet* condition for the outlet face.
d. Set *Symmetry* condition for those faces which represent the mirror image of the geometry.
e. Set *Fluid* zone for the volume(s) that represents fluid flow.
f. Set *Solid* zone for the volume(s) that represent the solid volume.

3. Checking the quality of grid

The grid can be checked for its quality in Gambit. Equiangle skewness, equisize skewness should be as small as possible, and must be below 0.9. Ideally, aspect ratio should be below 10, but having higher aspect ratios will still give accurate results, depending on the gradients in that direction.

APPENDIX B

CASE SETUP IN FLUENT

1. Importing Grid and Scaling

Once the grid is read into Fluent, it must be scaled to the actual units used when it was created in Gambit. Whatever the units in which the grid is created, Fluent takes the dimensions in SI units (m), and so appropriate scaling must be done to get the actual geometry dimensions. Also, grid check need to be done to make sure that there are no errors (skewness, zero volume and such) in the grid.

2. Setting the case

a. Appropriate models need to be selected like Laminar flow (default) and Energy Equation

b. Materials need to be selected. Standard materials like water can be copied from the Fluent database in the materials panel. The properties need to be edited, and set to the PCM slurry properties.

c. Boundary conditions need to be applied. The boundary conditions applied in Gambit are only for giving names to the boundaries. The actual specifications at the boundaries such as velocity, temperature, heat flux etc., need to be specified under the boundary conditions.

d. Solution controls need to be set appropriately. Solution controls consists of relaxation factors, first order and second order accuracy selection for the equations that are being solved. In general, the default under-relaxation factors are

good for obtaining a converged solution. If in case the solution diverges, these under relaxation factors need to be decreased (slowly) to get a converged solution. Also, it is better to get a converged solution using the first order accuracy option before using the second order accuracy option (since second order discretization is generally more unstable).

e. Residuals and Surface monitors need to be set to check the progress of the numerical simulation. Residual monitors show the convergence of continuity, momentum and energy equations. Surface monitors (for example, monitoring velocity and temperature at a point) show whether the flow is changing with iterations. In most cases, if the residuals have dropped to 1e-6, it means that the solution is not changing and the velocity and temperature at any point do not change with iterations. But the number 1e-6 is hypothetical and it is always better to ensure the flow convergence using surface monitor(s).

f. Initialize the solution.

g. Iterate till convergence.

APPENDIX C

POST-PROCESSING THE RESULTS

There are many options and ways of extracting results from Fluent. Contours, Vectors, Plots etc., are some examples of the different ways of viewing and extracting results from Fluent. Many variables like velocity, temperature, x-velocity, y-velocity, etc., can be plotted as contours, vectors or simple x-y plots. Before checking the results, it is necessary to create points, lines or rakes, surfaces etc., upon which the variables can be extracted. Many different tools like Iso-Surface, Iso-Clip, Point, Line/Rake can be used to create different surfaces for post-processing. In this study, Iso-Surface feature was used to create lines along the wall to calculate the average wall temperature and heat flux. Also, different types of averages, area-weighted average, mass-weighted average can be calculated. Some examples of the variables calculated in this study are explained below. It should be noted that the term "surface" does not only mean 2-D surface, "surface" can be a point, line or a 2D or 3D surface depending on how it is created:

a. To calculate the average heat flux from wall, it is necessary to create a line along the wall surface at that axial location. Using the Iso-Surface feature with constant grid-coordinate, and from the surface "wall", the line along the wall can be created. The average heat flux can be calculating the area-weighted average of total-surface-heat-flux along this line.

b. To calculate the bulk temperature, a surface on the fluid cross section is required. Again, the Iso-Surface feature with constant grid-coordinate can be used to create a cross sectional surface. Taking the mass-weighted average of temperature on this surface gives the bulk temperature at a given location.

c. To plot a variable along the center line of the domain, XY-Plot feature can be used. To get the XY-Plot, a rake surface is needed. Rake surface is a set of points along a straight line and it can be created by giving the start and end point coordinates, and the number of points required in between. Once the rake surface is created, XY-Plot of any variable (velocity, temperature etc.,) can be plotted for the rake surface.

APPENDIX D

CREATING JOURNAL FILES

Taking and calculating the average values at a specific location is simple. However, it is time consuming to get these values at several axial locations along the axial direction. Say for example, if 100 points are required to plot Nusselt number along the axial distance, 100 surfaces of each type, for example line (for wall average), cross sectional surface (for bulk temperature) etc., are needed. Creating hundreds of these surfaces one by one is tedious. In Fluent, there is a way to automate the process by creating Journal files consisting of TUI (Text User Interface) commands. The TUI commands are the commands that can be typed in the Fluent console, instead of using GUI (Graphical User Interface) menus like File, Display, etc. For example, an Iso-Surface can be created by GUI by going into Surface→ Iso-Surface from Fluent menu and entering the required parameters in the dialog box that opens. The same Iso-Surface can be created by using commands in the Fluent Console, by typing the following commands in the order,

a. Surface
b. Iso-surface
c. Grid-x-coordinate
d. X-coordinate
e. (Give the name of the surface)
f. (provide the surface from which it needs to be created, or leave blank)

g. (specify the zone, fluid/solid, from which the surface needs to be created, or leave blank)

h. (specify the limits, termed as iso-values)

By typing the above commands, the required surface can be created. All these commands can be typed into one line, instead of typing one after the other, by giving space in between them. The values that are left blank are indicated by comma (,) or closed brackets (()) in the line command. An example of the line command is given below.

Command : surf iso-sur z-coord surf-034 () (fluid) 1 ()

The above command creates a surface, named surf-034, at a z-coordinate of 1, out of the fluid domain, which results in a fluid cross section surface. This surface can be used to calculate the fluid bulk temperature. These one-line commands can be easily expanded to hundreds of commands by simply changing the numbers and names using Excel. Once the required commands are created in Excel, they need to be copied into a text document (say Notepad) and saved. This Notepad document can be saved and read into Fluent as a Journal File. When the Journal file is read into Fluent, all the commands will be performed, creating any number of surfaces/lines required.

VITA

Name: Satyanarayana Kondle

Address: C/O Dr. Jorge Alvarado

Department of Engineering Technology and Industrial Distribution

Texas A&M University

College Station, Texas 77843-3367

Email: satyam.iit@gmail.com

Education: B.Tech., Mechanical Engineering, Indian Institute of Technology Madras, India, 2007

M.S., Mechanical Engineering, Texas A&M University, 2010